Monte Carlo Simulations of Polymer Single Crystal: Morphology, Nucleation, and Melting

Jianing Zhang and Murugappan Muthukumar*

Polymer Science and Engineering Department,

Materials Research Science and Engineering Center,

University of Massachusetts, Amherst, MA 01003, USA

(Dated: October 31, 2007)

Abstract

A novel "anisotropic aggregation" model was proposed to simulate nucleation and growth of polymer single crystals as a function of temperature and polymer concentrations in solution. One of unusual assumptions adopted here is that prefolded whole chains serve as the smallest dynamical units in crystallization kinetics. This model solved the long-standing dilemma about kinetic and thermal roughening, by producing rough-flat-rough transition. It was found the crystal growth rate varied nonlinearly with temperature and concentration. The measured induction time and critical nucleus size conformed with experiments and gained deeper insight into the mechanism of nucleation. Melting temperatures as a function of crystal size, heating rate and concentration were also reported.

* Author to whom correspondence should be addressed. E-mail: muthu@polysci.umass.edu

I. INTRODUCTION

Classical crystallization of small molecules tends to form three-dimensional (3D) crystals. In contrast, polymers in solution or melt inevitably crystallize into a 2D crystal lamella with a thickness of about 10nm. It was found fifty years ago that polymer chains fold back and forth in the lamella [1]. This chain folding process, which was believed to occur concomitantly with the growth of polymer crystals, has been explicitly incorporated into most theories for polymer crystallization.

The most widely accepted theory for polymer crystallization hitherto is Lauritzen-Hoffman (LH) surface nucleation theory [4, 5]. It assumes the side surface of a thin lamella to be flat and serve as the growth front. A polymer chain with random-coil conformation will diffuse to the growth front and try to nucleate on it. The first stem of the chain attched on the growth front has to be longer than a critical value ($L > L^*$), in order to overcome the nucleation barrier created by an excess surface energy and a reduction in bulk energy. LH theory also assumes there are an ensemble of crystals, each having a different thickness and a growth rate which is determined by that thickness. The fastest growing crystals will form the majority and determine the average thickness L which is measured in experiments [4, 5]:

$$L = L^* + \delta L = \frac{A}{\Delta T} + \delta L \tag{1.1}$$

where A is a constant, δL is a small value in comparison with L. The supercooling ΔT is defined by $T_m^0 - T$, where T_m^0 is the equilibrium melting temperature of infinitely large crystals, and T is the isothermal crystallization temperature. Note the nucleation rate is nil when $L = L^*$, reaches the maximum at a finite thickness $L = L^* + \delta L$, and then decreases to a small value when $L \gg L^*$. Based on such a correlation between the nucleation rate and L, the growth of polymer crystals was assumed to be nucleation-controlled and therefore the growth rate G can be expressed by

$$G \propto \exp\left(\frac{-K}{T\Delta T}\right) \tag{1.2}$$

where G is the linear radial growth rate of lamellae and K is the nucleation constant. Later on, it was found that the plot of $\log G$ vs. $\frac{1}{T\Delta T}$ was not necessarily linear but showing a kink of slope change. So the concept of regime I→II transition was introduced [6], where the slope K fell off with lowering temperature. Interestingly, the reverse situation was also

found in experiments where the slope K rose up with lowering temperature. This latter effect was identified as regime II→III transition [7]. LH theory interpreted three regimes as a result of competition between surface nucleation rate i of the first stem and substrate completion rate g of subsequent stems [9]: Regime I at higher temperatures corresponds to a mononucleation region where $i \ll g$. The surface nucleation i is the rate-determining step and substrate completion is so rapid that the growth face tends to be flat; Regime II at intermediate temperatures corresponds to a multiple-nucleation region where $i \approx g$ and the growth front starts to show some roughness; Regime III at lower temperatures corresponds to a numerous-nucleation region where $i \gg g$ such that the niche separation is on the order of the stem width. Apparently the above analysis leads to a conclusion that the crystal outline becomes rougher at lower temperatures, a phenomenon known as "kinetic roughening". The slopes in three regimes were observed to obey the relation $K_{g(I)} = 2K_{g(II)} = K_{g(III)}$ [13], reflecting the underlying physics $G_I \propto i$, $G_{II} \propto i^{1/2}$, and $G_{III} \propto i$, which served as a strong support for regime transition theory. A list of experimental evidences for regime transitions can be found in the book [2] and the review article [9]. Most of regime transitions observed in experiments are I-II and II-III types. A full regime transition of III-II-I type has been found only in a few experiments [13, 14]. In particular, a reversion to regime II at the highest temperature, which shows III-II-I-II behavior, has also been observed in some cases [15, 16].

Although LH theory can account for temperature dependence of lamellar thickness L and crystal growth rate G to a certain degree, it still has many inherent deficiencies. The abrupt upswing of lamellar thickness L at large supercoolings, i.e. "δL catastrophe", was predicted by LH theory but never seen in any experiment [9]. Instead, the thickness reached a plateau at lower temperatures [11], which actually put the validity of Eq. 1.1 in serious question. Introducing an apportioning factor ψ ($0 < \psi < 1$) between forward and backward reactions [10] and choosing '$\psi = 0$' or 'low ψ' will eliminate δL catastrophe or shift δL catastrophe to sufficiently low temperatures. However, there is no a priori justification for arbitrary choice of ψ values used to produce a better fit to experimental data [2, 3]. The concept of regimes I, II and III was also questioned by Point and Janimak in terms of the unrealistic values of kinetic length which was defined by the ratio between substrate completion rate g and surface nucleation rate i [12]. Another problem with LH regime transition theory is that the slope change in the plot of $\log G$ vs. $\frac{1}{T\Delta T}$ is not concomitant with the morphological change at the same regime transition temperature [14, 39]. Lastly, LH theory can only account

for "kinetic roughening" phenomenon (roughness appeared at lower temperatures), but encounter difficulties in explaining "thermal roughening" phenomenon (roughness appeared at higher temperatures) [17]. In experiments, the axial ratio and curvature of polyethylene crystal outlines was observed to increase with temperature [38, 39], raising serious doubts on validity of LH nucleation theory at higher temperatures [17]. In light of this discrepancy, Miller and Hoffman introduced the concept of "lattice strain" into the {200} serrated sectors through a parameter σ_s to account for thermal roughening [8]. Nevertheless, lattice strain concept suffered from a fact that curved {200} sectors can be observed even in extended-chain polyethylene crystals [42], which was supposed to be free of lattice strain. Besides, it remains to be explained why and when σ_s (based on the serrated sector) takes over from σ (based on the flat sector) as the determining factor [3].

Inspired by thermal roughening phenomenon, Sadler and Gilmer applied the "rough surface growth theory" developed for crystal growth of small molecules to the case of polymers and proposed an alternative model for polymer crystallization, i.e. rough surface growth model combined with pinning effects (SG roughness/pinning model) [17–21]. The surface roughness on a molecular level was introduced to account for curved crystal outline at high temperatures. This thermal roughness requires that the binding energy between the smallest units in the crystal is comparable with kT [17], where k is Boltzman's constant and T is absolute temperature. As a result, the smallest unit was estimated to be a segment of polymer chain (ca. 6 $-CH_2-$) in SG model rather than a complete stem (ca. 800 $-CH_2-$) in LH theory. Sadler disputed the premise that surface nucleation is always the rate determining factor, arguing that nucleation may be a more important barrier at lower temperatures than at higher ones. However, for rough surface growth of small molecules, G is normally predicted to be linear with supercooling [17]:

$$G \propto \Delta T \tag{1.3}$$

whereas for a 'nucleation' type of growth it is of an exponential type conforming to Eq. 1.2. For polymers, G was known to follow Eq. 1.2. Based on this fact, Sadler and Gilmer introduced the pinning entropic barrier to replace the nucleation energy barrier in LH theory to account for this nonlinear temperature dependence [18]. The pinning barrier represents a trap created by crystallization of a stem shorter than L^* in Eq. 1.1. Further crystallization next to this short stem with a stem length longer than L^* has a big disadvantage due to

the expense for the creation of new side surfaces. Therefore crystallization is interrupted by the short stem, and the pinning stem has to be removed to resume the crystallization [19]. The growth rate limited by this pinning effect has the same exponential dependence on the supercooling as that limited by nucleation. The strong dependence has been explained as a result of increasing number of traps with the increase in stem length. In that sense, the pinning has been considered as an entropic barrier. By introducing pinning effects into rough surface growth, SG model can qualitatively reproduce the temperature dependence of both lamellar thickness L in Eq. 1.1 and growth rate G in Eq. 1.2 without invoking surface nucleation, as demonstrated by Monte Carlo simulations [18, 20] and rate equation approach [19, 21].

Unfortunately, SG roughness/pinning model did not provide an analytical theory to be tested in experiments. It is primarily qualitative, relying on computer simulations to provide evidence of the correct type of behavior [3]. The rate equation approach is only a numerical solution based on a row of stems which is cut out of the crystal perpendicular to the growth face, neglecting all lateral correlations. And the pinning concept becomes questionable since pinning should result in a tapered edge [20], which contradicts with the AFM observations on polyethylene single crystals [31, 32]. More importantly, SG model only takes thermal roughening into account, leaving kinetic roughening unexplained. This is in the opposite direction with LH theory where only kinetic roughening can be successfully explained. In the present study, our anisotropic aggregation (AA) model is able to produce both thermal roughening and kinetic roughening at the same time. It appears to us that nothing but the competition between the binding energies and thermal fluctuation kT is enough to produce rough-flat-rough transitions and nonlinear temperature dependence of G, without invoking surface nucleation concept or pinning effects.

Another important aspect which needs to be addressed is the effect of polymer concentrations in solution. Apparently the preceding theories failed to predict the observed concentration dependence. It is expected that the surface nucleation rate i is proportional to polymer concentration C and the substrate completion rate g is independent of C [3]. Hence the predicted concentration dependence in LH theory will be $G_I \propto C$, $G_{II} \propto C^{1/2}$, and $G_{III} \propto C$ for three regimes respectively ranging from high to low temperatures. In

experiments, the concentration dependence is generally expressed by [68]

$$G \propto C^{\alpha} \tag{1.4}$$

where α is a constant known as "concentration exponent". Experimental results revealed α depends on temperature [45, 68, 69], concentration [34, 68, 70], and molecular weight [69]. Normally α is in the range $\frac{1}{3} < \alpha < 1$ [2], with some extreme case where $\alpha > 1$ and could be as high as 2 [68]. The general trend for concentration exponent is that α increases with crystallization temperature T [45, 68]. And sometimes α would transit from a lower value to a higher one with decreasing C, exhibiting a kink in the plot of $\log G$ against $\log C$ [34, 68, 70]. The failure of LH theory in predicting concentration dependence inspired people to introduce cilia nucleation concept [71, 72] to account for the general trend of α, i.e. α increases with increasing T or decreasing C. The cilia nucleation will lead to $\alpha < 1$, while the nucleation of solute molecules from the solution will lead to $\alpha \geq 1$. So the competition between cilia and solute nucleation and their relative weight as a function of C and T will qualitatively explain the general trends of α. However, in the present paper, our AA model is also able to confirm these two general trends, without invoking the cilia nucleation concept.

Hitherto most theories for polymer crystallization assumed that chain folding occurs concomitantly with crystal growth, and therefore chain folding process has to be explicitly taken into account, as sketched in Fig. 1(a). Nevertheless, there is increasing evidence of the presence of nodular structures in polymer crystals [22], which can be traced back to forty years ago [23]. It suggested that there are paracrystalline nodules with partial order (or precursors) originally present in the amorphous phase. As Geil and Yeh speculated [23, 24], the crystallization might occur by movement, rotation, alignment and perfection of internal order of these paracrystalline nodules. Strobl proposed a four-step route of polymer crystallization from melt via mesomorphic ("hexagonal") and granular crystalline layers to lamellar crystallites [22]: attachment of chains from the isotropic melt onto mesomorphic layer → mesomorphic layer thickens → transit into granular crystal layer when reaching a critical thickness → merge into homogeneous crystal. On the other hand, recent simulations have demonstrated that a single polymer chain or multiple chains tend to self-nucleate to form a partially ordered structure (bundles or nodules) within a short period of time [25, 26]. When two such bundles come together, they will favor to be parallel with each other and the perpendicular configuration is simply unfavored in energy [25]. In addition, polymer

chains were observed in simulations to adsorb onto the growth front spontaneously without invoking any energy barrier [27], in direct contradiction with the nucleation-based LH theory.

Inspired by the above experiments and simulations, we proposed a two-step route for polymer crystallization shown in Fig. 1(b) and a new anisotropic model to simulate the step 2. In the step 1, upon quenching the system to lower temperature, it is assumed that polymer chains with random coil configurations will quickly self-nucleate to form paracrystalline bundles before polymer crystallization taking place. As shown in the previous simulations [25, 26], this spontaneous self nucleation might be driven by the competition between Van der Waals attractions of adjacent stems and the torsion/bending penalty of polymer chain backbone. In step 2, where polymer crystallization occurs, these paracrystalline bundles will random walk and aggregate to from a crystal via their anisotropic interactions. Note chains might increase their thickness L as time elapses or upon aggregation, according to simulation results. But this is assumed to have no influence on the aggregation kinetics. In summary, this new model is distinct from previous theories in at least four aspects:

1. The smallest dynamic unit is not one stem in LH theory or one segment in SG model, but the whole chain bundle.

2. The crystallite thickness is predetermined in step 1 and becomes irrelevant with the crystallization kinetics in step 2, contradicting with the concept that the growth rate G reach the maximum at a finite thickness L and the average thickness $< L >$ is determined by the fastest growth rate G_{max}.

3. The crystallization (adsorption) and melting (desorption) are fully reversible and the observed crystallization rate reflects their compensation, in a line with SG model but contradiction with LH theory. The adsorption of chains onto the growth front will gain energy (attractive interactions) so that the nucleation barrier in LH theory is not present.

4. A specific anisotropic interaction is introduced, distinct from the isotropic binding energy in SG model [18].

It should be mentioned that this model is very similar to the models for crystallization of small molecules except for the anisotropic interactions introduced here, which confines the growth of polymer crystals in a 2D plane and strongly contributes to the slowness of polymer crystallization kinetics.

The model and algorithm will be provided in the second part. Morphologies are given in the third part. The fourth part presents the effects of time, temperature, concentration and nucleus size. The discussion and conclusion will be given in the fifth and sixth part respectively.

II. MODEL AND SIMULATION ALGORITHM

We set up a new model with anisotropic local interactions to simulate polymer crystallization. This model can be categorized into Lattice Kinetic Monte Carlo method and Potts model, viz. the extension of Ising model from two states (spin up and spin down) to multiple states.

Simulations are performed in a huge cubic simulation box with length $100 \times 100 \times 100$ (viz. $L_{box} = 100$) under periodic boundary conditions, which is further discretized into 10^6 cubic lattices with length $1 \times 1 \times 1$. L_{box} varies from 100 to 500 in the present study. Each cubic lattice is assigned a state from five possible states, as shown in Fig. 2: state S_0, empty cubic lattice (or regarded as solvent); state $S_1 \sim S_3$, x, y, z-oriented free chain (prefolded bundle with partial order); state S_4, z-oriented crystalline chain serving as the nucleus for subsequent crystal growth.

The simulation procedure is as follows: $\langle 1 \rangle$ Put a few z-oriented nucleus (state S_4) at the center of the simulation box. $\langle 2 \rangle$ Put certain number ($L_{box}^3 \times C$) of free chains with random orientations (states $S_1 \sim S_3$) at random locations in the simulation box. $\langle 3 \rangle$ Randomly pick up one chain. Let it random walk and randomly change its orientation. $\langle 4 \rangle$ Calculate its energy state before (E_0) and after (E_1) such a random walk. Decide whether to accept such a random walk based on the acceptance probability in classical Metropolis algorithm:

$$P = \begin{cases} 1 & \text{when } \Delta E \leq 0 \\ \exp\left(\frac{-\Delta E}{kT}\right) & \text{when } \Delta E > 0 \end{cases} \tag{2.1}$$

where the energy change $\Delta E = E_1 - E_0$. Repeat step $\langle 3 \rangle$ and $\langle 4 \rangle$ for several billion times. The number of iteration is given in units of Monte Carlo step (MCS). At 1 MCS, the number of attempted random walks was equal to the total number of free chains in the simulation box. As is conventional for Monte Carlo simulations, a temperature parameter is taken as kT with units of energy rather than just temperature. The initial random configuration of free chains is to mimic the athermal state of polymer solution above melting temperature.

Then kT parameter is set to a constant value so that the whole process of simulation is to mimic an isothermal crystallization process at kT after quenching from above melting temperature.

The energy state is calculated by counting how many crystalline chains (state S_4) are in its 6 nearest neighbors and what interaction these neighbors give. Here the local anisotropic interaction is simply defined as the attraction ($E_p < 0$) between two neighboring parallel chains and the repulsion ($E_n > 0$) between two neighboring non-parallel (perpendicular or end-to-end) chains. Since only the ratio $\Delta E/kT$ is employed in calculating acceptance probability, we reduced E_p to unity and tried different kT values. It turned out that meaningful results are obtained only in the range $kT = 0.13 \sim 0.20$, below or above which the kinetics will be too slow or the crystal will not grow. After setting $E_p = -1$, for simplicity, we further set $E_n = +1$. Different magnitudes of $E_n = +1 \sim +5$ have been tried and the results showed no big difference as long as a certain repulsion existed to avoid non-parallel aggregation of chains. The following Eq. 2.2 gives a more specific definition of our energy setting:

$$\begin{cases} \text{parallel:} & E_{xy}(S_3, S_4) = E_{xy}(S_4, S_4) = -1 \\ \text{perpendicular:} & E_{xy}(S_1, S_4) = E_{xy}(S_2, S_4) = +1 \\ \text{end-to-end:} & E_z(S_1, S_4) = E_z(S_2, S_4) = E_z(S_3, S_4) = E_z(S_4, S_4) = +1 \end{cases} \tag{2.2}$$

where the subscript xy corresponds to 4 nearest neighbors along x and y directions; the subscript z corresponds to 2 nearest neighbors along z direction. Only the interaction with crystalline chains (state S_4) was considered, i.e. omitting interactions between free chains (state $S_1 \sim S_3$) to avoid forming multiple crystals. So the present study is focused on single crystal growth and to mimic heterogeneous nucleation in nature. In contrast, primary nucleation and multiple crystals growth will be the focus of another future paper.

The length scale for each lattice is around 10 nm, which is the typical value for lamellar thickness and nodular size [22, 23]. For polymer chains in dilute solution, the typical diffusion coefficient at volume fraction $C = 0.001$ was about $D = 10^{-7}$ cm^2/s [29, 30]. So the time scale for each MCS can be estimated as 10^{-5} s because $D = \frac{10^{-7}\ \text{cm}^2}{\text{s}} = \frac{(10nm)^2}{10^{-5}\ \text{s}}$. Thus a typical run in simulation with $t_{max} = 1 \times 10^7$ MCS will correspond to 100 seconds in reality. Nonetheless, we have to admit the above estimation of time scale is rather crude.

III. RESULTS

A. Morphologies

The most important point in this paper is concerning lateral habits of polymer crystals as a function of temperature and concentration. The study of Wunderlich *et al.* [33] showed that polyethylene grows from dilute o-xylene in the form of faceted lozenge-like crystals at 84℃ (see Fig. 3(3)). Below 80℃ the angle of the crystal apex becomes increasingly sharpened with decreasing temperature, leading to a sharpened-apex lozenge shape at 75℃ (see Fig. 3(2)). At even lower temperature $T_c < 74$℃, the crystals become more dendritic, resulting in a hedgehog dendrite habit (see Fig. 3(1)). The transition from faceting habit to sharpened-apex lozenge and then to dendrites indicated the transition of underlying mechanism from nucleation-controlled to diffusion-limited growth [34]. Free chains with random diffusion path will prefer to land on the outer region of the lozenge (the lozenge apex sticking out) rather than the middle part (screened by the apex), which results in sharpened apexes.

As is mentioned in the introduction, two types of flat-to-rough transition have been found in experiments [43]: one is at lower temperatures (kinetic roughening); the other one is at higher temperatures (thermal roughening). Kinetic roughening has been found in both solution and melt. As depicted in Fig. 3(4-5), Tanzawa [35] observed that the outline of the lamella grown from isotactic polystyrene solution transformed from a hexagon at 130℃ to a more rounded circle at 110℃. Yamashita *et al.* [36] also observed that the morphology of isotactic Poly(butene-1) in the melt film transformed from a square faceting shape at 100℃ to a rounded and wavy habit at 85℃. As mentioned previously, kinetic roughening has been explained as a result of $i \gg g$ in LH theory, where i is the surface nucleation rate and g is the substrate completion rate.

Alternately, thermal roughening was quantitatively investigated by Organ and Keller [38, 39]. At lower crystallization temperature T_c, the outline of crystals is a faceted lozenge with four straight {100} faces (see Fig. 3(6)). At higher T_c, two extra {100} faces appear and the crystal outline becomes truncated lozenge shape. The length of the {100} face and the curvatures of both {100} and {110} faces increase with T_c regardless of solvent. At the highest T_c, the crystal becomes rounded and elongated, as shown in Fig. 3(7). In literature,

at least four types of mechanism have been proposed to account for the rounding of habits at higher temperatures: (1) "lattice strain" in serrated {200} faces [8]; (2) the substrate completion is interrupted by impurities (branching, lower-molecular-weight component, or adsorbed solvent) [41]; (3) inherent defects in crystals formed by the boundaries of small domains with distinct stacking [9, 42]. (4) equilibrium thermal roughening when the binding energy ϵ between the smallest units becomes comparable with kT [17]. The first mechanism, i.e. lattice strain caused by chain folding, was ruled out by the fact that extended-chain crystals also exhibited rounded habits [42]. The effect of impurity caused by low-molecular-weight component will not be the main reason either, because curved habits were also observed with monodisperse polyethylene. Our simulation results are in favor of the last mechanism, i.e. rounding caused by thermal roughening ($\epsilon \approx kT$). Toda criticized the thermal roughening mechanism based on a speculation that thermal roughening should result in an isotropic outline [42]. He was in favor of the third mechanism (defects in crystals), and speculated that the anisotropy of the habits can be explained if the excess energy required for crossing the boundaries of small domains (viz. defects) on a {200} face is larger than the energy on a {110} face. However, as pointed out by Organ and Keller [38], the anisotropy of habits might also arise from the anisotropic binding energy between molecules along {110} and {200} faces. If introducing anisotropic binding energies along x,y directions into our model, it will be no surprise to produce anisotropic morphologies. Actually this further modification to our model is a future work for us, which might also help to realize the sectorization of single crystals. Thus it appears to us the anisotropy of habits can not be an adequate reason to rule out the thermal roughening mechanism.

The intermediate part in Fig. 3 presents our simulation results at three different concentrations. With increasing temperature and lowering concentrations, the crystal outline experienced five different types of habits: dendritic structure $\rightarrow$ sharpened-apex lozenge $\rightarrow$ kinetic roughening $\rightarrow$ faceting $\rightarrow$ thermal roughening. At high concentration $C = 0.004$ and low temperature $kT = 0.100$, the crystal outline is dendritic, as shown in Fig. 3(8). At intermediate concentration $C = 0.0005$ and low $kT = 0.090$, a sharpened-apex single crystal is formed (Fig. 3(9)). At low concentration $C = 0.00002$, a well-defined faceting is formed at intermediate temperature $kT = 0.135$ (Fig. 3(11)). At the same dilute concentration, the rounding habits caused by kinetic roughening (Fig. 3(10)) or thermal roughening (Fig. 3(12)) will show up at lower or higher temperature respectively.

The lower part of Fig. 3 gives schematic representations of crystal outlines observed in experiments. By comparing the upper, intermediate and lower parts in Fig. 3, the one-to-one correspondence between simulation results and experimental photos is clearly seen. The difference of habits between Fig. 3(3) and (11) is because the smallest unit in simulations is in a square shape rather than a lozenge shape in experiments. This problem can be solved by a proper coordination transformation of the square shape in Fig. 3(11) to the lozenge shape in Fig. 3(3). It should be mentioned that the sharpened-apex lozenge shape in Fig. 3(9) is commonly seen in many experiments and might be termed differently as right-angle dendrites [33] or lozenge with sharpened points [34]. In these five types of habits, you might consider the dendritic structure and sharpened-apex lozenge as the extreme cases of kinetic roughening. In fact, with decreasing temperature, a faceted polystyrene crystal can transform into either a rounded habit (in the thicker film) or a dendritic structure (in the thinner film) [37], indicating the close relationship between these two habits. However, this classification is deemed inappropriate because the former two morphologies are diffusion-controlled in nature while kinetic roughening should belong to interface-controlled mechanism [3].

Fig. 4 presents a full landscape for crystal habits, equally-spaced temperatures and concentrations being x and y-axis. The bold solid line delineate the boundary for dissolution transition, showing phase diagram behavior for polymer crystallization. It appears that the dissolution temperature T_d increases logarithmically with concentration, leveling off at higher concentrations. If shifting this bold line toward left, all morphologies along the solid line are similar, indicating that morphologies (or roughness transitions) are influenced by both temperature and concentrations. For example, at $kT = 0.12$, the habit gradually transforms from rounded shape to sharpened-apex lozenge shape when the concentration is raised from 0.00005 to 0.00065. The rounded habit at $kT = 0.12$ and $C = 0.00005$ is more like the morphology at $kT = 0.16$ and $C = 0.00065$. In addition, along each solid line, the habit becomes more faceting with decreasing concentrations. This conclusion is important because it is not only consistent with Keith's observations that axial ratios will increase with concentrations [40], but also explains why the regularly faceted lozenge shape is only available in very dilute solutions [2, 42]. At $C = 0.00050$ in Fig. 4, starting from a lower temperature to a higher one, the habit transits from sharpened-apex lozenge ($kT = 0.10$) to a wavy habit ($kT = 0.12$), then to a rounded habit caused by kinetic roughening ($kT = 0.14$), and at last to the rounding habit caused by thermal roughening ($kT = 0.20$). Note there is

no well-defined faceting at this intermediate concentration so that it is hard to tell whether the rounding is caused by kinetic or thermal roughening. This problem can be settled at a very low concentration $C = 0.00002$, where a well-defined faceting is formed at intermediate temperature $kT = 0.135$, as shown in Fig. 5. At such a low concentration, kinetic roughening and thermal roughening is well separated by the faceting habit. Another difference between thermal and kinetic roughening is that thermal roughening at high temperatures tends to have much more free chains hanging around (manifested by the shrinkage of size of the crystal at C=0.00050 and kT=0.22 in Fig. 4) and adsorption/desorption occur more frequently so that its shape become more fluid and varies from time to time.

Fig. 6 showed time evolution of five typical habits. A common feature is that the habits do not change much during growth. To confirm this, we did quantitative measurements of roughness, in a similar way as that defined in Ref. [17]. The only difference is that the roughness definition in Ref. [17] is focused on double or multilayer models and essentially a roughness on the fold surface, while ours is the roughness on the lateral surface of monolayer lamella. Anyway, the roughness parameter (RP) is defined as the number of bonds parallel to the surface which are broken as a fraction of the number of surface lattice sites:

$$RP = \frac{n_1 \times 3 + n_2 \times 2 + n_3 \times 1}{n_1 + n_2 + n_3} \tag{3.1}$$

where n_i is the number of crystallites who has i crystallites as neighbors. For example, n_1 represents the number of 1-neighbor crystallites who reside on the flat growth front and have one neighboring crystallite and three unbonded sides facing the solvent (only the four sides along x,y directions are considered in measuring the roughness on the lateral surface). n_2 and n_3 are referred to the crystallite in the corner and the middle of growth front respectively. n_4 represents the crystallite in the inner part of the lamella and is not considered here, since the roughness measured here is only on the surface. n_0 should correspond to the free chains who has all four sides along x,y directions facing the solvent. Ideally, the complete faceting should correspond to the case where all edge crystallites are 3-neighbor cases except four corner crystallites who are 2-neighbor cases. Assuming the lamella is large enough to neglect the contributions of four corner crystallites, the complete faceting should lead to $RP = \frac{n_3 \times 1}{n_3} = 1$. If rotating the faceted habit 45 degree to a complete serrated habit, resembling the sharpened-apex habit, the resulted roughness should be $RP = \frac{n_2 \times 2}{n_2} = 2$. The thermal roughening habit should correspond to the mixture of 2-neighbor and 3-neighbor cases, and

therefore the resulted RP is expected to be around 1.5. Through the measurements of RP for morphologies in Fig. 4 and 5, it is found the roughness normally decreases a little bit at early stage of growth and then reach equilibrium at late stage (figure not shown here). And the late-stage roughness at higher temperatures tends to fluctuate in larger magnitude than that at lower temperatures. The average values of roughness parameters at late stage are depicted in Fig. 8. Three important features are evident, in accordance with previous arguments: rough-flat-rough transition with increasing temperatures; the lower concentration, the more faceting; the roughness transition also depends on concentrations. Now the reason why RP decreased with time at early stage becomes clear in the sense that the instantaneous concentration of free chains also decreased with time. Fig. 8 also explained why faceting is only available in dilute solution within a narrow temperature range [45]. It also need to be clarified why RP values never exceed 1.5 and reach the ideal value of 2 even for the massively-serrated habit, i.e. the sharpened-apex lozenge. By zooming in the edge of sharpened-apex lozenge, it is found the outline is not completely serrated on a single site level. There are many small plateau of two or three sites wide, leading to many 3-neighbor crystallites.

B. Time evolution of lamellar size

Fig. 9 and 10 present the time evolution of crystal radii as a function of the initial nucleus size (nu), temperature (kT) and concentration (C). The lamellar radius R (viz. the distance between the lamellar center and edge) is defined as a half of root square of the number of crystalline chains: $R = \frac{\sqrt{\mathrm{n_c}}}{2}$, by assuming the crystal lamella in a square shape. A common feature in two figures is that R increases approximately linearly with time at early stage and then level off to an equilibrium value at late stage due to the depletion of free chains, in good agreement with experimental observations [44, 45]. The initial growth rate G appears to decrease with increasing temperature (see Fig. 9) or decreasing concentration (see Fig. 10). At the highest temperature or lowest concentration, there emerges an additional stage, induction (or nucleation) stage, before the linear growth stage, where the crystal is observed to grow and resolve back until its size fluctuation is large enough to overcome the nucleation barrier. For this case, the plot of R vs. *time* can be separated into three stages: (1) induction or nucleation stage; (2) linear growth stage; (3) equilibrium stage.

The length of the induction stage is normally called "induction time" τ, which is defined as the time at which crystallization becomes detectable. By comparing Fig. 9(a) with (b), it is evident that τ increases more dramatically with kT for $nu = 7\times7$ than for $nu = 1\times1$ (this behavior will be elaborated in the ensuing section). τ approaches infinity at $kT = 0.170$ and $kT = 0.200$ for $nu = 1 \times 1$ and $nu = 7 \times 7$ respectively, indicating there is a temperature gap $kT = 0.170 \sim 0.200$ where small nucleus of the size 1×1 can not grow while large nucleus of the size 7×7 can easily grow. The same argument applies to Fig. 10 too, where there is a concentration gap $C = 0.00003 \sim 0.00019$. Imagine some experiments happen to be within such gaps, then there will be three ways to accelerate the nucleation process from infinite long time to an instant: (1) putting in a bigger heterogeneous nucleus (i.e. seeding technique) (2) increasing polymer concentrations (3) lowering temperature. It appears to us that decreasing concentration has similar effects as increasing temperature, which reinforces the previous conclusion that effects of temperature and concentration are strongly correlated. Obviously, the initial nucleus size nu will have no influence on stage (2) and (3). Once the nucleation barrier has been overcome, the subsequent growth should follow the same growth law no matter what nu is, since the subsequent crystallites after the crystal size becomes larger than 7×7 will feel no difference between $nu = 1 \times 1$ and $nu = 7 \times 7$.

Regarding the final equilibrium stage where R reaches the equilibrium value R^e, it can be seen from Fig. 9(b) that R^e keeps constant in low-kT region and then decreases dramatically with temperature in high-kT region, in accordance with the shrinkage of lamellar size and increasing numbers of free chains in Fig. 4 ($C = 0.00050$ & $kT = 0.22$). It appears to us that stage (3) of polymer crystallization resembles the equilibrium stage of chemical reactions, in the sense that reversible crystallization and melting occur frequently at high temperature and finally compensate with each other to reach an equilibrium.

The degree of crystallinity is defined by the number of crystalline chains divided by the total number of chains: $\Phi_c = \frac{n_c}{n_{all}} = \frac{(2R)^2}{n_{all}}$. For the case $L_{box} = 200$, $C = 0.00020$ and $nu = 1 \times 1$, the total number of chains is a constant $n_{all} = 200^3 \times 0.00020 + 1 \times 1 = 1601$. Fig. 11 showed time evolution of the crystallinity. As a result of only one lamella present in the simulation box, the crystallinity Φ_c becomes proportional to the square of lamellar radius: $\Phi_c \propto R^2$. So no wonder Fig. 11 looks very similar to Fig. 9(a). Due to one-to-one correspondence between Φ_c and R, there is no need to give more figures regarding Φ_c. Wang investigated the crystallization kinetics of polyethylene from deuterated o-xylene

solutions by time-resolved small-angle neutron scattering [46]. Uniquely in his measurement, both the increase of crystallinity and the decrease of volume fraction of free coil chains are monitored simultaneously. Both results are consistent with Fig. 11 in three aspects: As the crystallization temperature T_c is raised, the induction time τ becomes longer, the slope of Φ_c vs. *time* becomes lower, and the final equilibrium value of crystallinity Φ_c^e becomes lower too.

Fig. 12 showed the temperature dependence of the equilibrium number of crystallites n_c^e, which is proportional to the equilibrium crystallinity Φ_c^e. For the case $L_{box} = 200$ and $C = 0.00020$, the equilibrium crystallinity Φ_c^e is equal to $\frac{n_c^e}{1601}$, $\frac{n_c^e}{1609}$ and $\frac{n_c^e}{1649}$ for the nucleus size of 1×1, 3×3 and 7×7 respectively. So if Fig. 12 is replotted with Φ_c^e as y-axis, the three curves will completely overlap on each other, indicating the final equilibrium state is independent on the initial nucleus size. The only difference is that small nucleus $nu = 1 \times 1$ can only grow up to $kT = 0.165$ while large nucleus $nu = 7 \times 7$ can grow up to higher temperature $kT = 0.195$. Another feature is that $\Phi_c^e = 1$ at lower temperatures and then decreases exponentially with temperature, revealing the equilibrium size of the crystal is smaller at higher temperatures. Alternatively, the amount of polymers in solution (i.e. $1 - \Phi_c^e$) will increase sharply with temperature, a feature confirmed by the experiment (see Fig. 26 and Table 9 in Ref. [47]).

C. nucleation and induction time

Fig. 13 showed the time evolution of morphologies during the initial nucleation process at high temperature $kT = 0.196$, where the crystal is observed to grow and resolve back until its size fluctuation happens to exceed a critical nucleus size r_c. After $r > r_c$, the crystal will have greater tendency to grow than to shrink. In this case, r_c appears to be between $\frac{\sqrt{73}}{2} = 4.3$ and $\frac{\sqrt{90}}{2} = 4.7$. Another feature in Fig. 13 is that the shape of the initial nucleus varies from time to time and is very rough and irregular in most time, rather than a regular square shape. This is consistent with the final morphology at $time = 1560 \times 10^4$ MCS but contradictive with the concept of classical nucleation theory, where the shape of nucleus is assumed to be regular (sphere in 3D non-lattice model or square in 2D lattice model) as a result of the minimization of surface tension. Similar observations of irregular nucleus shape has been found in the 2D simulations by Binsbergen [48] and in the real-space imaging of

nucleation of colloidal crystallization [49].

Due to the size fluctuation as high as $n_c = 73$ in Fig. 13, we made a program to automatically measure the induction time τ as the time when the total number of crystallites $n_c \geq 100$. For the case $C = 0.00020$ and $L_{box} = 200$ in Fig. 11, this is equivalent to set the induction time τ as the time when the degree of crystallinity reaches 0.06, i.e. $\tau = t_{\frac{100}{1601}} = t_{0.06}$. For very rare cases (normally at larger nu and the highest kT) where the size fluctuation is even larger than 100, we measured the true induction time manually. Because of single nucleus and the randomness of size fluctuation, the measured induction time τ is different with different random number seeds (In contrast, the induction time for multiple primary nucleation is an average result and expected to be less undulatory). Fig. 14 presents the τ distributions averaged on 50 different random number seeds. Obviously τ distribution is a log normal distribution and becomes broader at higher temperatures.

The average values of τ with huge error bars of standard deviation were depicted in Fig. 15(a) as a function of temperature. At low temperatures, τ reaches a nonzero constant value. The existence of nonzero value is due to the fact that we measured τ as the time at which the total number of crystallites $n_c \geq 100$. So even for the case of no induction time, it still takes some time for n_c to reach 100. Therefore each curve in Fig. 15(a) should be shifted downward a little bit to make the nonzero constant region become zero. Anyway, our major ensuing conclusions would not be impaired even without such a minor modification. First, it is evident that induction time increases dramatically with temperature. This is no surprise since almost all measurements of crystallinity on polymer systems will exhibit such a behavior [2, 50]. The surprise comes from the influence of the initial nucleus size nu. At higher nu, it seems that the curve of τ vs. kT shifts to higher temperatures. And the shift distance becomes smaller as nu increases evenly. It tends to approach a limit value $kT = 0.21$ when $nu \to \infty$. $kT = 0.21$ is more like a true equilibrium melting temperature, at which the crystal can not grow even without any nucleation barrier ($nu \to \infty$). A third feature is that the increase of τ with kT becomes much sharper at higher nu so that a finite induction time only occurs in a narrower temperature range (e.g. $kT = 0.13 \sim 0.165$ for $nu = 1 \times 1$; $kT = 0.185 \sim 0.2$ for $nu = 7 \times 7$). The beauty of our model is that we can specify the size of initial single nucleus, which allows us to deduce the critical nucleus size r_c via measuring the induction time. For example, at $kT = 0.17$, the induction time τ for $nu = 1 \times 1$ approaches infinity while τ for $nu = 3 \times 3$ is only 64×10^4 MCS. This means

at such a temperature $kT = 0.17$, the crystallites can never grow on a 1×1 nucleus but can quickly grow on a 3×3 nucleus, which leads to a conclusion that the critical nucleus size satisfies $1 < r_c < 3$ at $kT = 0.17$. In an alternative way, the transition temperature between the regions with short and with long induction times can be measured for each nu. Here we arbitrarily set the transition point as the intersects between horizontal line $\tau = 100$ and each curve in Fig. 15(a). For example, the horizontal line $\tau = 100$ intersects the curve of $nu = 5 \times 5$ at the transition temperature $kT = 0.189$. Namely $kT = 0.189$ corresponds to the critical nucleus size $r_c = 5$, because at this temperature $kT = 0.189$ the nucleus of $r < 5$ will take very long induction time $\tau \gg 100$, and the nucleus of $r > 5$ will take very short induction time $\tau < 100$. By this way, we plot the critical nucleus size as a function of temperature in Fig. 15(b). It is clearly seen that r_c increases dramatically with kT and tends to diverge at a limit $kT \approx 0.21$ (melting temperature). The arbitrary choice of horizontal line $\tau = 100$ will not impair the major features in Fig. 15(b), as long as the curve in Fig. 15(a) shifts to higher temperature and the shift distance becomes smaller when nu increases evenly. It should be mentioned such a nonlinear dependence of r_c on kT is fully consistent with theoretical predictions [51].

Another surprise comes from the influence of polymer concentration C on induction time and critical nucleus size, as shown in Fig. 16. Again, four features are evident: (1) τ decreases with increasing C. (2) at bigger nu, the curve of τ vs. C shifts to lower C. (3) as nu increases evenly, the shift distance becomes smaller and tends to approach a limit value of $C \approx 0.00004$. (4) at bigger nu, the increase of τ with lowering C becomes sharper so that finite τ values are discernable in a narrower concentration range. Similarly, as shown in Fig. 16(b), r_c increases dramatically with lowering concentration and tends to diverge at $C \approx 0.00004$. The above results again reinforce the previous argument that the effects of temperature and concentration are strongly correlated and increasing temperature is similar to lowering concentration. To our knowledge, there is very little information in literatures regarding the concentration influence on induction time for polymers. And the effect of concentration on nucleation process has been almost totally neglected by polymer scientists. So the results presented in Fig. 16 need to be tested in the measurements of crystallinity for polymer solutions. However, the dependence of nucleation on concentration is not new for researchers in the field of biopolymer crystallization. For example, the induction time will increases with either increasing temperature or decreasing concentrations for crystallization

of lysozyme solution [52]. It has been well known in the field of biopolymer crystallization that the induction time is a function of supersaturation and by definition supersaturation is closely related to both temperature and concentration.

D. Melting temperature

Before measuring lamellar growth rates, the knowledge of undercooling and melting temperature T_m is a must for the purpose of testing Eq. 1.2. It is well known that T_m depends on a number of factors, including crystallization time t_c, crystallization temperature T_c, heating rate β and polymer concentration C in the case of polymer solutions. Here we focus on the last three factors and exclude the effect of t_c by running simulations long enough time to reach equilibrium states, i.e. $t_c \to \infty$. After crystallinity Φ_c reaches its equilibrium Φ_c^e, the system is heated up at a constant heating rate and the variation of crystallinity is monitored. The temperature at which the last trace of crystallinity disappears is taken as T_m.

Firstly, as shown in Fig. 12, the final equilibrium size of crystal decreases with increasing crystallization temperatures, which means we could vary R by adjusting T_c. It is expected that larger crystals will melt at higher melting points, conforming to Gibbs-Thompson equation [58]:

$$T_m = T_m^0 \left(1 - \frac{const}{R}\right) \tag{3.2}$$

where T_m^0 is the equilibrium melting temperature for infinite large crystals, and R is the crystal size. Normally R refers to the lamellar thickness for polymer crystals and this relation has been widely utilized to extrapolate T_m^0. Here in our model, the crystal thickness is not a variable and R stands for the lateral size of lamella. This relation should work as well because a lamella of smaller size has a larger curvature and therefore is apt to melt at lower temperature. Fig. 17 presents the plot of T_m versus $1/R$. It is evident that a linear relation is satisfied. Nevertheless, the extrapolation of T_m^0 is impracticable since this relation is strongly dependent on heating rate β too. At the fast heating rate $\beta = 50 \times 10^{-8}$/ MCS, the extrapolation of the T_m vs. $1/R$ data to $1/R = 0$ will give $T_m^0 = 0.32$. At intermediate heating rate $\beta = 10 \times 10^{-8}$/ MCS, the slope becomes shallower and T_m^0 is estimated as 0.27. At the slowest heating rate, the linear line becomes almost flattened and $T_m^0 = 0.22$.

The effect of β on the Gibbs-Thompson plot is not surprising for us, since similar be-

havior has been seen in the plot of T_m vs. $1/L$ (inverse of lamellar thickness), where with increase of β, the Gibbs-Thompson plot shifted upward (see Fig.21(b) in Ref. [60] or Fig.2 in Ref. [59]) and its slope becomes steeper (see Table III in Ref. [59]). Furthermore, the fact that T_m becomes independent on T_c (or R) when the heating rate is extremely slow has long been recognized, which was actually called "slow stepwise warming technique" [54]. T_m thus obtained is well-defined, reproducible, and independent of any previous thermal history of the sample [61]. Such a fact has been cited as an evidence that the melting temperature obtained by slow heating was in fact the true equilibrium melting temperature. Our simulations support this view. Although T_m^0 is not available, we can still measure the true melting temperature (T_m^{true}) which is independent of T_c. To us, the behavior in Fig. 17 can be explained by the following arguments. At higher heating rate, it takes longer time for larger crystals than smaller crystals to melt **layer by layer**. The longer melting time, the higher melting point. This is a typical "superheating" phenomenon when supplying more heat to the crystal than the crystal can melt. For very slow heating, there will be plenty of time for both large and small crystals to melt layer by layer. And at each stepwise temperature during slow heating, the crystal size has plenty of time to reach its equilibrium size. So both types of crystals will melt at the same temperature for slow heating.

To quantify the above results, T_m is plotted against heating rate β in Fig. 18. It is found that T_m increases logarithmically with β, which is a typical result of superheating effects [55]. At the slowest heating rate $\beta = 1 \times 10^{-8}$/ MCS, $T_m = 0.218$ defines the upper limit of T_m^{true}. Following the trend of the curve, T_m^{true} should be even lower. Another way to delimit T_m^{true} is to crystallize isothermally for very long time. It is found that the crystal growth occurs only if $kT \leq 0.198$. At $kT = 0.200$, the crystal grows and shrinks back and forth, indicating the competition between crystallization and melting is balanced. This temperature can serve as the lower boundary for T_m^{true}. So we roughly estimated $T_m^{true} = 0.21 \pm 0.01$. On the other hand, superheating effects have been prevailingly quantified by the relation $T_m \propto \beta^n$, where n is normally equal to 0.5 [62], but in rare cases equal to 0.20 [60], or 0.23 [63]. The inset in Fig. 18 showed that $n = 0.29$ for the present case. The discrepancy is unclear for us. However, our preliminary simulations on melting of multiple crystals (instead of single crystal here) have led to $n = 0.5$, which suggests that introducing competitions between multiple crystals may alter the value of the exponent n from 0.29 to 0.5.

Although T_m^{true} is independent of T_c, it should still be a function of initial polymer con-

centration C. The more crystalliable polymers, the higher tendency for crystallization. By adding more polymers into the system, the balance between crystallization and melting is broken so that the system has to be heated to even higher temperature to re-establish a new balance between both sides. This is the reason for concentration dependence of T_m^{true}. Fig. 19 presented the depression of T_m at dilute concentrations. It is seen that T_m decreases rapidly with decreasing concentration in the dilute region. Similar effects of solution concentration on T_m have been found in low-molecular-weight polyethylene fractions in xylene solutions (Fig. 3 in Ref. [56]) and small molecules in a good solvent, in agreement with Flory's theory on melting point depression [57].

E. Lamellar growth rate

It has been widely accepted that the lamellar growth rate G for polymer solutions is constant with time, except for the late stage when polymer chains in solutions become exhausted [44, 45]. Although this argument appears to be true for Fig. 9 and 10 at first sight, more accurate measurements of time derivative of R in Fig. 9 and 10 showed that the growth rate is NOT constant with time even at the early stage. Note such a high accuracy in measuring instantaneous growth rates is not available in experiments due to scarcity of data points. As demonstrated in Fig. 20, G gradually decreases with time because the concentration of free chains are decreasing too. At higher concentration, such a decrease of G with time becomes more prominent. At dilute condition, G looks more constant with time except that at the very beginning it increases slightly due to the existence of induction time (presumably the initial slight increase of G occurs when the lamellar size is so small that it is hardly detected in experiments, especially for the "self-seeding" technique where the initial nucleus size is very big). A similar argument may apply to effects of temperature as well. As temperature is raised, the small peak in the curve of G vs. *time* becomes more flattened and shifts to longer time scale. Again, increasing temperature has a similar effect on G as decreasing concentrations. The point is that the conditions of higher temperature and lower concentration are favorable for G to "appear" constant with time, although G is never constant in a strict sense but exhibits a broad and flattened peak. Finally, it should be stressed that the decrease of G with time as a result of material depletion is not a new concept for solution-grown crystals. An isochronous decoration technique has been

employed to measure the quasi-instantaneous growth rate and G is observed to decrease when crystallization proceeds further [64, 65]. The optical micrographs of isotactic polystyrene crystals grown from concentrated solutions also showed that G is initially constant and then decreases with time [66].

The variation of G with time makes it difficult to choose an appropriate range of time over which G should be measured, since choosing a different range will lead to a different G value. To measure G in a consistent way, we judged the range visually by the criterion that the linear regression line did not deviate from data points too much. And then the same procedure was repeated 50 times for different random-number seeds and the average value of G thus obtained should have better accuracy. Fig. 21 presents the temperature dependence of lamellar growth rate G at various concentrations. A common feature is that G decreases with temperature nonlinearly, although G seems proportional to ΔT in the low and high temperature regions. As mentioned in the Introduction, the nonlinear dependence of G on T has been attributed to either the secondary nucleation barrier or pinning entropic barrier, leading to the derivation of Eq. 1.2. The above two barriers, however, are apparently nonexistent in our model, and consequently a different explanation is of necessity (see the Discussion). Note the y-axis in Fig. 21 is in a linear scale. Most experimental results presented G in a logarithmic scale and showed a downward curvature [8, 39, 42]. However, if those G data in Ref. [8, 39, 42] are extracted and replotted in a linear scale, the curve of G vs. T will show an upward curvature, contrary to that in Fig. 21.

The reason for such a discrepancy is still unclear. But three possible reasons have emerged. First, the upward curvature of G vs. T is often observed in a narrow temperature range (ca. 10 Celsius degree) just below the melting point. This will correspond to $kT = 0.195 \sim 0.200$ in the case of $C = 0.0002$ in Fig. 21, assuming that $T_m = 140$℃ corresponds to $T_m = 0.20$ in our model. So our simulation results showed an overall trend over a very large temperature range. In fact, Toda and Kiho studied crystal growth of polyethylene solution and their G vs. T data (Table II in Ref. [34]) showed a downward curvature, as shown in the inset of Fig. 21. Note these data were obtained at very high supercoolings and in very dilute solutions, both of which are necessary conditions for a direction comparison with our simulation results. Toda and Kiho attributed the leveling off of G at high supercoolings to the transformation from a nucleation-controlled mechanism to a diffusion-limited one. At very high supercoolings, they found the crystal habit becomes a sharpened-point

lozenge and G depends linearly on concentration, in good agreement with our simulation results. The second possible reason might be the "self-seeding" technique widely employed by most experimenters, where crystallization starts from large crystal nuclei instead of the smaller ones employed in our simulations. The third possibility is due to the competition between multiple crystals. This would be future work for us, although our present model is merely focused on a single crystal without considering any inter-crystal interaction.

In order to test Eq. 1.2 of LH theory, we replotted the $C = 0.0002$ data from Fig. 21 in the form of $\log G$ versus $1/T(T_m^0 - T)$, as shown in Fig. 22. Note the data points for $kT < 0.14$ are not included, since including them will unrealistically bend the left part of the curve upward or even rightward. This suggests the linear dependence of G on ΔT at low temperatures in Fig. 21 might correspond to an ideal but unrealistic case, where heterogenous nucleation still dominates at such high supercoolings. Our preliminary study on primary nucleation has shown that G will decline with decreasing temperature and exhibit the well-known "bell" shape, when the competition between multiple crystals is introduced. Since T_m^0 is unavailable from the Gibbs-Thompson plot in Fig. 17, we replace T_m^0 in Eq. 1.2 by $T_m^{true} = 0.21$ and the curve thus obtained is essentially linear, lending good support to LH theory. However, as Hoffman and Weeks pointed out [54], the T_m obtained by slow warming technique is at least a few degrees below T_m^0. So different values of T_m^0 have to be tried for Eq. 1.2. The other two curves in Fig. 22 correspond to $T_m^0 = 0.203$ and 0.25 respectively. For clarity purpose, both curves are shifted upward or downward slightly along y-axis. For $T_m^0 = 0.203$, the plot of $\log G$ vs. $1/T\Delta T$ shows an upward curvature. If it is divided into two regimes, the slope of the low-T region, $K_1 = 0.0025$, will be twice the value of the slope in the high-T region, $K_2 = 0.0012$. For $T_m^0 = 0.25$, the reverse situation occurs and $2K_1 = K_2$.

It appears to us that the plot of $\log G$ vs. $1/T\Delta T$ depends on the choice of T_m^0. As T_m^0 increases, the curve will transit from an upward curvature to a linear line, and then to a downward curvature. At the same time, the slope K will increase with T_m^0 too. The above dependence of both regimes and K on the choice of T_m^0 is fully consistent with many experimental observations [44, 67, 68]. Eq. 1.2 seems to merely be a good fitting function to growth rate data if only a good choice of T_m^0 is made, especially when considering that T_m^0 values for most polymers (e.g. PP and PEO) bear large uncertainty. This finding objects the regime-transition theory based on Eq. 1.2, which has been further questioned by other

experimental observations.

According to regime transition theory, regime I-II-III transitions are caused by a change in the kinetic length, and such change should also cause a kinetic roughening transition in morphologies. However, a paradox has been reported on crystallization of isotactic polystyrene in solutions and melt [35, 66], and isotactic polybutene in the melt [36]. While the morphology transits from a faceted to a rounded habit with decreasing temperature, the plot of $\log G$ vs. $1/T\Delta T$ does not show any transition. On the other hand, for thermal roughening, Organ and Keller found that there is no discontinuous changes in morphology (quantified by the curvature and axial ratio) at the regime transition temperature which is determined by the kink in the plot of $\log G$ vs. $1/T\Delta T$ [39]. The same situation occurred to our simulations. The original data in Fig. 21 shows that G varies continuously with kT, especially at the regime transition temperature $kT = 0.18$ which is extracted from either the upper or lower curve in Fig. 22. The smooth transition of G with kT should originate from the smooth transition of morphologies with kT in Fig. 4. This supports our view that Eq. 1.2 is merely a good fitting function, and any kink generated by Eq. 1.2 does not necessarily correspond to any abrupt change in the underlying nucleation mechanism or kinetic length. The second point against regime transition theory is due to unrealistic values of kinetic length [12]. Point *et al.* [64] pointed out that the kinetic length of the magnitude estimated is potentially visible in the electron microscope, which was not seen in experiments [39]. The third objection comes from values of the slope K and the associated surface energy term $\sigma\sigma_e$. Tanzawa found the slope K was four times as large as the value predicted by nucleation theory [35]. Miyamoto *et al.* [66] and Keller *et al.* [68] found that the slope K increases with decreasing polymer concentration, contradicting with the intuition that surface energies $\sigma\sigma_e$ should be independent on concentration. Indeed, if plotting $\log G$ vs. $1/kT(0.21 - kT)$ for two other concentrations, the result will be $K_1 = 0.015, K_2 = 0.025$ for $C = 0.00005$ and $K_1 = 0.002, K_2 = 0.0005$ for $C = 0.00035$. By comparing with $K = 0.0034$ for $C = 0.00020$ in Fig. 22, it is readily seen that K increases with decreasing C. So using a unique T_m^0 in Eq. 1.2 for G data at various concentrations becomes inappropriate. Doing so will not only result in dramatic change of slope K and associated $\sigma\sigma_e$, but also make the plot of $\log G$ vs. $1/T\Delta T$ become curved, thus generating an additional regime. To maintain a constant $\sigma\sigma_e$ value at various concentrations, the best choice of T_m^0 for a linear fit of $\log G$ vs. $1/T\Delta T$ is $T_m^0 = 0.187, 0.213, 0.223$ for $C = 0.00005, 0.00020, 0.00035$ respectively. In

this case, K varies little and is equal to 0.0046, 0.0044, 0.0039 accordingly. This finding questions the validity of using a unique T_m^0 value in Eq. 1.2 and the definition of quenching depth $\Delta T = T_m^0 - T$. The dependence of best choices of T_m^0 on C reminds us of the T_m dependence on C shown in Fig. 19. So T_m^0 in Eq. 1.2 has to be replaced by T_m as a function C, in order to maintain a constant and meaningful surface energy term $\sigma\sigma_e$. Finally, it should be mentioned that the data in Fig. 22 are not two intercepting straight lines, in a strict sense, but an smooth curve. This phenomenon has been noted by Cooper and Manley as well [69] .

Regarding the concentration dependence of G, it is widely accepted that $G \propto C^\alpha$, where α is a constant normally ranging from 1/3 to 1 [34, 45, 69, 70], with some exceptions where α is as high as 2 [68]. Fig. 23 presented our simulation results for the concentration dependence of G. It is clearly seen that $\alpha = 1$ at low temperatures or at high concentrations, indicating that G is proportional to C when the underlying mechanism for crystal growth is diffusion-limited aggregation. At higher temperatures or lower concentrations, α shows a transition from 1 to 2 or even higher values. As Keller and Pedemonte suggested [68], $\alpha = 2$ means that an attachment event requires simultaneous arrival of 2 chains onto the growth front. There is much higher tendency for a single chain to leave the flat growth front, unless another chain arrives timely to stabilize both chains. On the other hand, the immediate implication of the weak concentration dependence ($\alpha < 1$) is that chains are being hindered in their attachment to the crystal face, which might stem from the shielding of the crystal face by an adsorption layer, or simply from the competition between cilia nucleation and solute chain nucleation [68]. Unfortunately, we did not observe $\alpha < 1$ behavior in our simulations. The reason for this discrepancy is still not clear at present.

Although the magnitude of α values we obtained are generally larger than the normal values seen in experiments, the results presented in Fig. 23 revealed several important trends which are fully consistent with those in experiments. First, α increases with decreasing concentration [34, 68, 70]. Second, α increases with increasing temperature [45, 68, 69]. Third, all curves at various temperatures converge at higher concentrations [68], which means that at a sufficiently high concentration G becomes less dependent on temperature. Fourth, at lower temperatures, the crystal growth can take place at even lower concentrations [34, 70]. Finally, a new feature is revealed only by our simulation data with improved accuracy due to the average over 50 runs. It is found that α is NOT a constant in a strict sense, since α

apparently varies smoothly with concentration, which further makes the validity of Eq. 1.4 become questionable. On the contrary, Toda *et al.* argued that as concentration decreases α transforms from 0.5 to 1 with a kink in the plot of $\log G$ vs. $\log C$ [34, 70]. And the crossover concentration at the kink point is independent of temperature. However, more careful look on the raw data in their figures reveals no apparent kinks but smooth curves. Even if such kinks exist, the crossover concentration should be temperature dependent as deduced from Fig. 23.

IV. DISCUSSION

A. reversible crystallization/melting and mechanism of five habits

Our model questioned the traditional concept that polymer crystal growth is nucleation-controlled and once-formed crystallites will never resolve back. Fig. 24 revealed that the apparent growth rate is determined by the competition between reversible crystallization and melting. As suggested by experimental results, at higher temperatures the recrystallization rate could be 1000 times faster than the apparent growth rate.

Fig. 25 schematically illustrated the dependence of recrystallization/remelting rates on both temperatures and concentrations. It is expected that the adsorption is proportional to concentration but independent on temperature, due to the fact that adsorption probability is always unity no matter how many neighbors it will have (because the energy is always gained $\Delta E < 0$). Meanwhile, the desorption rate will be independent on concentration but strongly dependent on temperature and local environment (how many neighboring crystallites it has). As shown in upper part of Fig. 25, recrystallization will be the same at the same concentration. Nonetheless, the desorption rate will increases dramatically with temperature as a result of the desorption probability $P = e^{\frac{-\Delta E}{kT}}$. So it is the compensation between adsorption and desorption rather than the nucleation barrier which leads to nonlinear dependence of G on kT.

On the other hand, the interaction between ΔE and kT in the expression of $P = e^{\frac{-\Delta E}{kT}}$ determines the five different habits:

1. At the lowest temperature, the dendritic structure is formed quickly and some of interface crystallites belong to one-neighbor case (i.e., it has only one neighboring crystallite). This

means the once-formed crystallites are very stable and the probability of desorption is almost zero, even for one-neighbor case. For example, at $kT = 0.10$, the desorption probability is $P_1 = e^{\frac{-1}{0.10}} = 4.5 \times 10^{-5}$ and $P_2 = e^{\frac{-2}{0.10}} = 2 \times 10^{-9}$ for one-neighbor and two-neighbor case respectively. The low desorption probability leads to a lateral habit determined only by diffusion path of free chains.

2. At a little higher temperature, $kT = 0.14$, the desorption probability becomes higher for both $P_1 = e^{\frac{-1}{0.14}} = 7.9 \times 10^{-4}$ and $P_2 = e^{\frac{-2}{0.14}} = 6.2 \times 10^{-7}$. At this temperature, one-neighbor case becomes unstable but two-neighbor case is still stable, which leads to the habit of sharpened-angle lozenge.

3. At even higher temperature, $kT = 0.16$, two-neighbor case becomes unstable but three-neighbor case is still stable, which leads to faceted lozenge shape.

4. At $kT = 0.18$, three-neighbor case becomes unstable but four-neighbor case is still stable. Thus the interface of crystal becomes unstable so that the habit of crystals varies from time to time showing large fluctuations. Thermal roughening is reached.

5. At $kT = 0.20$, even four-neighbor case become unstable. The desorption rate becomes comparable or larger than the adsorption rate so that the whole crystal melts (or crystal growth can not occur).

6. At $kT = 0.15$, the transition habit between sharpened-angle lozenge (2-neighbor case) and faceted lozenge (3-neighbor case) will be kinetic roughening (coexistence of 2-neighbor and 3-neighbor case).

On top of the effect of temperature on habits, concentrations also influence habits by adjusting the adsorption rate. From Fig. 25 it is seen that more adsorption events will occur at higher concentrations, which will make the crystallites on the growth front have less chance to get out before other free chains landing and overwhelming it. Because of overwhelming effects, the crystallites on the growth front will have less time to rearrange themselves into a more regular and faceted habit (from 1,2-neighbor cases to 3-neighbor case). Therefore the roughness of crystal outline increases with concentrations.

B. mechanism of nucleation and surface energy

The nucleation process is obviously present in our simulations. It is observed from Fig. 13 the crystal grows and resolves back until its size happens to exceed the critical nucleus size. As illustrated in Fig. 15 and 16, the smaller the nucleus size is, the longer induction time it will take to grow crystals. There is a temperature region where smaller nucleus can not grow while larger nucleus can grow easily. In this sense, this temperature region can be called nucleation-controlled region. Traditionally, it is believed that the nucleation barrier comes from the competition between bulk energy and surface energy. However, the surface energy is zero in our simulations (the interaction between crystallites and solvent is zero). It appears to us that the competition between the bulk energy (the interaction between two crystallites) and kT is enough to produce the nucleation process. This puzzle will be resolved by Fig. 26. As two schematic examples, the nucleus size of 3×3 and 5×5 are compared to show the mechanism of nucleation and surface energy. Here the crystallites of 4-neighbor case (in the inner part) are almost impossible to desorb so that we only focus on the desorption of surface crystallites. Apparently the desorption probabilities of surface crystallites depend on the local binding energies with other crystallites. The average binding energy $\langle\varepsilon\rangle$ for surface crystallites of size R will be

$$\langle\varepsilon\rangle = \frac{(4R-8)\times 3 + 4\times 2}{4R-4} = 3 - \frac{1}{R-1} \tag{4.1}$$

where $(4R-8)$ is the number of surface crystallites of 3-neighbor case and 4 is the number of corner crystallites. The total number of surface crystallites will be the sum of both $(4R-4)$. So the average binding energy of surface crystallites of $nu = 3\times 3$ and $nu = 5\times 5$ in Fig. 26 will be $\langle\varepsilon\rangle = \frac{4\times 3+4\times 2}{4+4} = 2.5$ and $\frac{12\times 3+4\times 2}{12+4} = 2.75$ respectively. This means the surface crystallites of $nu = 5\times 5$ have stronger binding energy than those of $nu = 3\times 3$ so that the former is much stabler than the latter. As the nucleus size increases, it is expected from Eq. 4.1 that $\langle\varepsilon\rangle$ will become saturated and approach the limiting value 3. In another word, increasing nucleus size from 1×1 to 3×3 will make much more difference than increasing nucleus size from 3×3 to 5×5, as evidenced by Fig. 15 and 16. Another way to address this issue is to calculate the average desorption probability for surface crystallites:

$$P_{desorb} = \frac{(4R-8)\times \exp\left(\frac{-3}{kT}\right) + 4\times \exp\left(\frac{-2}{kT}\right)}{4R-4} \tag{4.2}$$

After inputting some kT value, Eq. 4.2 showed that P_{desorb} decreases exponentially with increasing R. This means for small nucleus size the desorption probability is so high that the crystal growth can not occur.

At the first look, the mechanism presented here can be reconciled with the traditional arguments based on the surface energy, since the larger nucleus size the more surface area. The free energy of formation of the crystal of size R from the solution is

$$\Delta G = R^2 \times \Delta\mu - (4R - 8) \times \sigma_1 - 4 \times \sigma_2 \tag{4.3}$$

where the bulk energy is $\Delta\mu = 4$, surface energy for 3-neighbor case is $\sigma_1 = 1$, and surface energy for corner crystallites is $\sigma_2 = 2$. So $\Delta G = 4R^2 - 4R$. After setting its derivative to zero, we could obtain $R_c = 1/2$, a ridiculous result. In light of this, the traditional arguments that critical nucleus size is determined by the competition between bulk and surface energy is not applicable to our simulations. The incoming flux (adsorption events) which is proportional to concentration has been ignored by this traditional argument. Our simulations showed that the mechanism of nucleation is based on the competition between desorption and adsorption events. The former increases dramatically with decreasing nucleus size and that is the reason why nucleation occurs.

The adsorption events per unit time should be proportional to number of available free chains and available landing sites: $\frac{dn_a}{dt} = C \times 4R$. The desorption events per unit time should be proportional to number of surface crystallites and their desorption probability: $\frac{dn_d}{dt} = (4R - 8)\exp\left(\frac{-3}{kT}\right) + 4\exp\left(\frac{-2}{kT}\right)$. Combining both together and assuming $\frac{dn_a}{dt} = \frac{dn_d}{dt}$ at critical nucleus size R_c, we could obtain

$$R_c = \frac{2\exp\left(\frac{-3}{kT}\right) - \exp\left(\frac{-2}{kT}\right)}{\exp\left(\frac{-3}{kT}\right) - C} \tag{4.4}$$

From this equation it is seen R_c increases with increasing kT or decreasing C, consistent with Fig. 15(b) and 16(b).

Following the same way, we could calculate the growth rate as

$$\frac{dn_a}{dt} - \frac{dn_d}{dt} = \frac{d(R^2)}{dt} = RC - R\exp\left(\frac{-\langle\varepsilon\rangle}{kT}\right) \tag{4.5}$$

so the lamellar growth rate becomes

$$\frac{dR}{dt} = C - \exp\left(\frac{-\langle\varepsilon\rangle}{kT}\right) \tag{4.6}$$

This equation can be used to extract the exact expression for $\frac{dR}{dt}$ since the current concentration C is also depends on R. By simply assuming $\frac{dR}{dt} = 0$ at melting point, we could obtain

$$T_m \propto \frac{-1}{\log C} \tag{4.7}$$

which has been confirmed by fitting our data from Fig. 19. The equilibrium crystallinity can be also derived by setting $\frac{dR}{dt} = 0$:

$$\Phi_c = 1 - C = 1 - \exp\left(\frac{-\langle\varepsilon\rangle}{kT}\right) \tag{4.8}$$

which shows an exponential decrease with kT in agreement with Fig. 12.

V. CONCLUSIONS

An anisotropic adsorption model (belonging to Potts model) is proposed for polymer crystallization, which is distinct from previous LH nucleation theories and SG roughness/pinning model in several aspects.

1. The smallest dynamic **unit is the whole chain** in our model, instead of the stem (80 CH_2 units) in LH theories [4, 5] or the segment (6 CH_2 units) in SG model [17, 18]. In contrast to two previous models, chain folding and crystal growth in our model do not occur simultaneously, but by two steps. The first step is the whole chain folds by itself to form a prefolded nodular structure, with a partial orientation order. The second step is the aggregation of those prefolded chains in the way the same as do the small molecules except anisotropic interactions introduced here. Our simulations are merely focused on the second step.

2. The second difference is the growth kinetics are independent on the crystal thickness L in our model, where apparently L **is always constant**. In contrast, LH theories assumes an ensemble of crystals with a range of thickness, each of which have a uniform L. All crystals have to satisfy the condition $L > L^*$, where L^* is the critical thickness for 1D nucleation. The average thickness $\langle L\rangle$ is chosen based on the kinetic consideration that the growth rates are faster for thin crystals at $L = L^* + \delta L$, and therefore that thin lamellae dominate the ensemble. On the other hand, SG model assumes the thickness fluctuation even in individual crystal. And nucleation is not invoked since $L < L^*$ is also

allowed in the pinning process. SG model also claimed that the growth rate reaches the maximum at finite thickness $L = L^* + \delta L$ and the crystal growth is kinetically controlled. The difference between LH theories and SG model is the former invoked a high enthalpy barrier from 1D nucleation process while the latter introduced a low entropy state by pinning effects. The consistence of our simulations with experiments put a question on all the considerations based on the crystal thickness and the nature of whether the polymer crystallization is kinetically controlled or thermodynamically driven.

3. **Anisotropic interactions** between prefolded chains are introduced into our model, which is believed to be the main distinction between polymer crystallization and small molecules crystallization. The anisotropic interaction confined polymers crystallizing into a 2D lamella. The confined geometry obviously will slow down the kinetics of polymer crystallization as well as melting, in comparison with those of small molecules. Although SG model also introduced a binding energy between units as ours, the interactions between segments are basically isotropic, resulting the roughness both on the lateral surface and fold surface.

4. Another feature, the same as in SG model but distinct from LH theories, is that the **reversible melting and crystallization** is automatically allowed in Potts model. The crystallization (adsorption) is always gaining energy and thus occurs smoothly without invoking any nucleation barrier: adsorption possibility $p = 1$. The melting (desorption) accompanies with an energy loss which is critically dependent on the local environment (2-neighbor case or 3-neighbor case) and absolute temperature: desorption possibility $P = \exp(-\Delta E/kT)$. In some senses, the polymer crystallization in our model is believed to be **desorption-controlled**, rather than the nucleation control in LH theories or pinning control in SG model. In addition, the rearrangement of crystallites along the growth surface is found to play a critical role in determining the lateral habits and roughness transitions at various temperatures, which was omitted by both LH and SG models.

Based on the above distinct assumptions for there models, the analytical or simulation results are also different.

1. In terms of crystal habits, LH theories based on faceted growth front (regime I) was extended to regime II [6] and regime III [7] at low temperatures to take into account the

kinetic roughening. The competition between nucleation rate i and the substrate completion rate g determines the three regime, which put a great difficulty to understand the emerging phenomena of thermal roughening at high temperatures. SG model proposed the thermal roughening concept when the binding energy is in the same order of magnitude of kT. However their explanations of thermal roughness are based on pinning effects rather than the competition between local binding energy ΔE and kT. In addition, their simulation results showed roughness both on lateral surface and fold surface. Even for the 2D projection of 3D structures in SG model, the faceting habit at low temperatures is not well-defined [20], in comparison with our clear roughness transition along the crystal outline. Moreover, simulation results by SG model only showed thermal roughening transition as increasing temperature, leaving kinetic roughening at low temperatures unexplained. In contrast, our model reproduced almost the full landscape along different temperatures and concentrations. Faceting crystal at dilute solution, thermal roughening at high temperatures, and kinetic roughening at lower temperatures are all clearly demonstrated. Our model even extended the morphologies to even lower temperatures, where the sharpened-apex single crystal and dendritic structures are observed and fully consistent with experiments.

2. In terms of the temperature dependence of the radial growth rate G, our simulations showed nonlinear decrease of G as a function of absolute temperature T. The smooth curve of G vs. T revealed the smooth transition of lateral habits during different temperatures, reinforcing the questioning on the regime transition arguments and reconciling the paradox why the correspondence between the transition of growth rates and morphologies are absent in many experiments.

3. Another important result is regarding the concentration effects, which has been omitted by most researchers. It is found that the concentration effect is strongly correlated with the temperature effect with regard to their collaborative influences on later habits. The well known relation $G \sim C^{\alpha}$ was examined by our simulations in details. It is confirmed of experimental observations that α increases with increasing temperature or decreasing concentrations. However, high accuracy in simulation results make us realize the α is actually not a constant in most cases, but smoothly change with concentrations.

4. In contrast to LH theories and SG model, our anisotropic adsorption model make it

possible to simulate the initial nucleation process. The effects of nucleus size on growth kinetics, together with the induction time as a function of nucleus size, temperature and concentrations, were studied in details. The results obtained agree with experimental observations and arouse new insight on the mechanism of nucleation and surface energy.

5. Several other features are also obtained. The traditional view that lamellar growth rate is constant with time has been questioned. The nonlinear dependence of melting temperature on concentration is suggested.

From the above descriptions, it is clear that our model extensively extend our scope of measurements and influence factors to a wider range. The good consistence between our model and experiments put many serious questions on existing concepts and theories in various aspects. In polymer community, the well accepted 1D nucleation theory ($L > L^*$) and SG roughness/pinning model need be reexamined. The rate-limiting process might not be nucleation or pinning, but the desorption (melting) process since nucleation (or absorption) is automatically allowed. This new concept can also reconcile the contradiction between slow nucleation rate and round lateral shape found in polymer crystallization at high temperature. The competition between absorption and desorption will result in a transition from non-equilibrium state (upon quenching) to an equilibrium state, alike to chemical reactions. In this sense, our model is an equilibrium model while both LH and SG models are kinetic models, where thickness is kinetically determined by the maximum growth rate. The well known equation $\log G \sim \frac{1}{T(T_m^0 - T)}$ might be only a good empirical fitting to experimental data. You can always choose suitable T_m^0 to obtain a straight or curved line. The regime transition theory based on this curved line becomes unreliable too. Since only absolute temperature is involved in our simulations, the traditional concept about T_m^0 and the supercooling ΔT driving force need be reexamined. This could explain the existence of large differences in G at the same δT but different T_c since the roughness of the face, and hence the growth rate, would be only dependent on absolute temperature T_c [39]. Obtaining T_m^0 through Gibbs-Thomphson relation is unreliable since it is heating rate dependent. The true T_m can be obtained by extremely slow heating though.

For physics community, the nucleation process and its theory need be revisited. Even without invoking surface energy, we can still observe the nucleation process. And more importantly, the effects of incoming flux and concentrations play an critical role in deter-

mining the nucleation process, which has been omitted completely. Nucleation depends on not only on temperature but also concentrations, viz. depends on supersaturation [53]. The induction time can be served as a good tool to measure the critical nucleus size R_c. We also showed that the nucleus can be composed by the same crystallites as the large crystal. The shape of nucleus is often rough rather than faceted. The competition between bulk energy and surface energy is not the true reason for nucleation. For people who are interested in roughness transition, the surface roughening temperature T_R where roughening transition occurs should also be concentration dependent. At high enough concentrations, only one roughening transition will be seen. At dilute concentration, another faceting habit will show up at intermediate high temperature, which separates the roughening into kinetic roughening and thermal roughening. At high temperature, the crystal habit is no longer stationary and its outline fluctuates within short period of time.

put polymer crystallization into the general framework of crystallization of small molecules.

question traditional R_c and competition between surface and bulk free energy. propose that competition between kT and surface binding energy, the latter strongly depends on R.

single secondary and self nucleation. nucleus is not necessarily smooth.

The final state of crystals are not trapped in an non-equilibrium state, but in real equilibrium.

The outline of nucleus is rough, non-equilibrium. G is determined not by ΔG of nucleation, but by the parameters governing attachment and detachment.

Acknowledgments

Acknowledgment is made to the National Science Foundation (Grant No. DMR 9970718) for support of this research and to the Materials Research Science and Engineering Center at the University of Massachusetts.

---

[1] A. Keller, Philos. Mag. **2**, 1171 (1957).

[2] J.M. Schultz, *Polymer Crystallization: The Development of Crystalline Order in Thermoplastic Polymers*, Oxford University Express (2001).

[3] K. Armitstead and G. Goldbeck-Wood, Adv. Polym. Sci. **100**, 219.

[4] J.I. Lauritzen and J.D. Hoffman, J. Res. Natl. Bur. Stds. **64A**, 73 (1960);

[5] J.D. Hoffman and J.I. Lauritzen, J. Res. Natl. Bur. Stds. **65A**, 297 (1961).

[6] J.D. Hoffman, L.J. Frolen, G.S. Ross, and J.I. Lauritzen, J. Res. Natl. Bur. Stds. **79A**, 671 (1975).

[7] J.D. Hoffman, Polymer **24**, 3 (1983).

[8] R.L. Miller and J.D. Hoffman, Polymer **32**, 963 (1991).

[9] J.D. Hoffman and R.L. Miller, Polymer **38**, 3151 (1997).

[10] J.I. Lauritzen and J.D. Hoffman, J. Appl. Phys. **44**, 4340 (1973).

[11] D.H. Jones, A.J. Latham, A. Keller and M. Girolamo, J. Polym. Sci.: Polym. Phys. **11**, 1759 (1973).

[12] J.J. Point and J.J. Janimak, J. Cryst. Growth **131**, 501 (1993).

[13] J.P. Armistead and J.D. Hoffman, Macromolecules **35**, 3895 (2002).

[14] S.Z.D. Cheng, J.J. Janimak, A. Zhang, and H.N. Cheng, Macromolecules **23**, 298 (1990).

[15] S.Z.D. Cheng, J. Chen, and J.J. Janimak, Polymer **31**, 1018 (1990).

[16] P.J. Phillips and N. Vatansever, Macromolecules **20**, 2138 (1987).

[17] D.M. Sadler, Polymer **24**, 1401 (1983).

[18] D.M. Sadler and G.H. Gilmer, Polymer **25**, 1446 (1984).

[19] D.M. Sadler and G.H. Gilmer, Phys. Rev. Lett. **56**, 2708 (1986).

[20] D.M. Sadler, Polymer **28**, 1440 (1987).

[21] D.M. Sadler and G.H. Gilmer, Phys. Rev. B, **38**, 5684 (1988).

[22] G. Strobl, Eur. Phys. J. E **3**, 165 (2000).

[23] G.S.Y. Yeh and P.H. Geil, J. Macromol. Sci.(Phys.), **B1**, 235 (1967); **B1**, 251 (1967).

[24] P.H. Geil, J. Macromol. Sci.(Phys.), **B12**, 173 (1976).

[25] C. Liu and M. Muthukumar, J. Chem. Phys. **109**, 2536 (1998)

[26] M. Muthukumar and P. Welch, Polymer **41**, 8833 (2000).

[27] P. Welch and M. Muthukumar, Phys. Rev. Lett. **87**, 218302 (2001)

[28] M. Muthukumar, Adv. Chem. Phys. **128**, 1 (2004).

[29] H. Fujita, *Polymer solutions*, Elsevier Science Pub. (1990).

[30] E.J. Amis and C.C. Han, Polymer **23**, 1403 (1982).

[31] Y. Ryousho, S. Sasaki, T. Nagamura, A. Takahara, and T. Kajiyama, Macromolecules **37**,

5115 (2004).

[32] S. Hocquet, M. Dosiere, A. Thierry, B. Lotz, M.H.J. Koch, N. Dubreuil, and D.A. Ivanov, Macromolecules **36**, 8376 (2003).

[33] B. Wunderlich, E.A. James and T.W. Shu, J. Polym. Sci.: Part A **2**, 2759 (1964).

[34] A. Toda and H. Kiho, J. Polym. Sci.: Polym. Phys. **27**, 53 (1989).

[35] Y. Tanzawa, Polymer **13**, 2659 (1992).

[36] M. Yamashita, H. Miyaji, A. Hoshino, and K. Izumi, Polym. J. **36**, 226 (2004).

[37] K. Taguchi, H. Miyaji, K. Izumi, A. Hoshino, Y. Miyamoto, and R. Kokawa, Polymer **42**, 7443 (2001).

[38] S.J. Organ and A. Keller, J. Mater. Sci. **20**, 1571 (1985).

[39] S.J. Organ and A. Keller, J. Polym. Sci.: Polym. Phys. **24**, 2319 (1986).

[40] H.D. Keith, J. Appl. Phys. **35**, 3115 (1964).

[41] A. Toda, J. Phys. Soc. Japan **55**, 3419 (1986).

[42] A. Toda, Polymer **32**, 771 (1991).

[43] H. Miyaji, Y. Miyamoto, K. Taguchi, A. Hoshino, M. Yamashita, O. Sawanobori, and A. Toda, J. Mater. Sci. **B42**, 867 (2003).

[44] V.F. Holland and P.H. Lindenmeyer, J. Polym. Sci. **57**, 589 (1962).

[45] D.J. Blundell and A. Keller, J. Polym. Sci.: Polym. Lett. **6**, 433 (1968).

[46] H. Wang, J. Polym. Sci.: Polym. Phys. **42**, 3133 (2004).

[47] D.A. Blackadder and H.M. Schleinitz, Polymer **7**, 603 (1966).

[48] F.L. Binsbergen, Kolloid Z. Z. Polym. **237**, 289 (1970).

[49] U. Gasser, E.R. Weeks, A. Schofield, P.N. Pusey, and D.A. Weitz, Science **292**, 258 (2001).

[50] L. Mandelkern, J. Appl. Phys. **26**, 443 (1955).

[51] A. Peterlin, Makrom. Chem., **74**, 107 (1964).

[52] J. Drenth and C. Haas, Acta Cryst. **D54**, 867 (1998).

[53] A.M. Kulkarni and C.F. Zukoski, Langmuir **18**, 3090 (2002).

[54] J.D. Hoffman and J.J. Weeks, J. Res. Natl. Bru. Stand. (U.S.) **A66**, 13 (1962).

[55] E. Hellmuth and B. Wunderlich, J. Appl. Phys. **36**, 3039 (1965).

[56] A. Prasad and L. Mandelkern, Macromolecules **22**, 914 (1989).

[57] P.J. Flory, *Principles of Polymer Chemistry*, Cornell University Press: Ithaca and London, 568, (1953).

[58] B. Wunderlich, *Macromolecular Physics*, Academic Press: New York, Vol. **3**, (1980).

[59] H. Marand and J.D. Hoffman, Macromolecules **23**, 3682 (1990).

[60] K. Yamada, M. Hikosaka, A. Toda, S. Yamazaki and K. Tagashira, Macromolecules **36**, 4790 (2003).

[61] D.E. Roberts and L. Mandelkern, J. Am. Chem. Soc. **77**, 781 (1955).

[62] J.E.K. Schawe and G.R. Strobl, Polymer, **39**, 3745 (1998).

[63] A. Toda, M. Hikosaka and K. Yamada, Polymer, **43** 1667 (2002).

[64] J.J. Point, M. Ch. Colet, and M. Dosiere, J. Polym. Sci.: Polym. Phys. **24**, 357 (1986).

[65] M. Tian, M. Dosiere, S. Hocquet, P.J. Lemstra, and J. Loos, Macromolecules **37**, 1333 (2004).

[66] Y. Miyamoto, Y. Tanzawa, H. Miyaji, and H. Kiho, Polymer **12**, 2496 (1992).

[67] N. Ding and E.J. Amis, Macromolecules **24**, 3906 (1991).

[68] A. Keller and E. Pedemonte, J. Crystal growth **18**, 111 (1973).

[69] M. Cooper and R.S.J. Manley, Macromolecules **8**, 219 (1975).

[70] A. Toda, H. Miyaji and H. Kiho, Polymer **27**, 1505 (1986).

[71] I.C. Sanchez and E.A. Dimarzio, Macromolecules **4**, 677 (1971).

[72] A. Toda, H. Kiho, H. Miyaji, and K. Asai, J. Phys. Soc. Jpn. **54**, 1411 (1985).

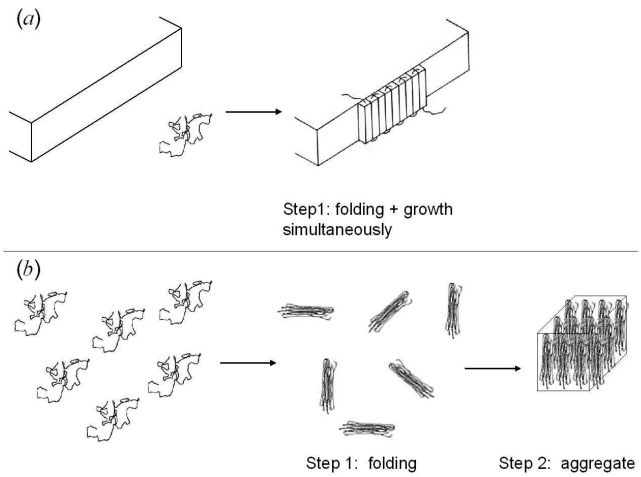

FIG. 1: chain folding and crystal growth occur (a) simultaneously in traditional theories; (b) via two steps in the present study.

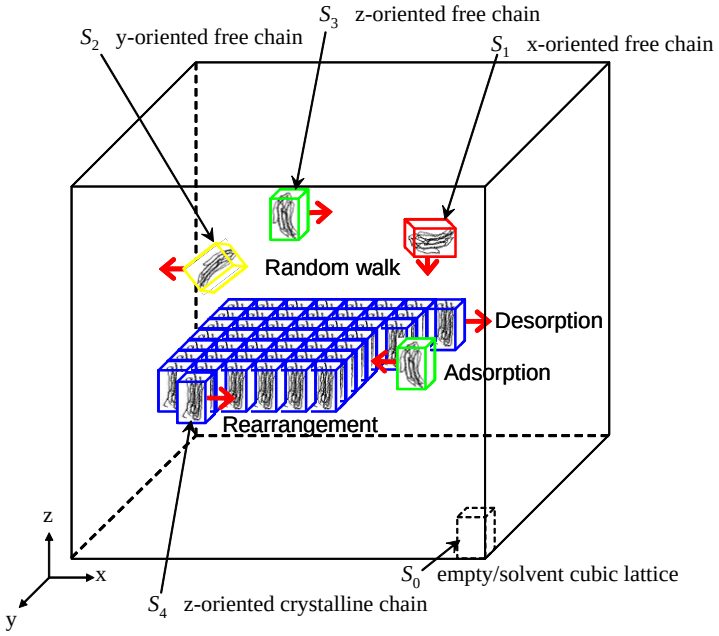

FIG. 2: Polymer solutions for single crystal growth is mapped onto a 3D array of lattice sites. Each lattice will take one of five possible states. S_4 serves as the nucleus. $(S_1 \sim S_3)$ and S_4 are interconvertible by adsorption and desorption. No interactions between free chains are allowed in order to form "single" crystal. For clarity purpose, the empty/solvent site S_0 is invisible here except one example shown at the right-bottom corner.

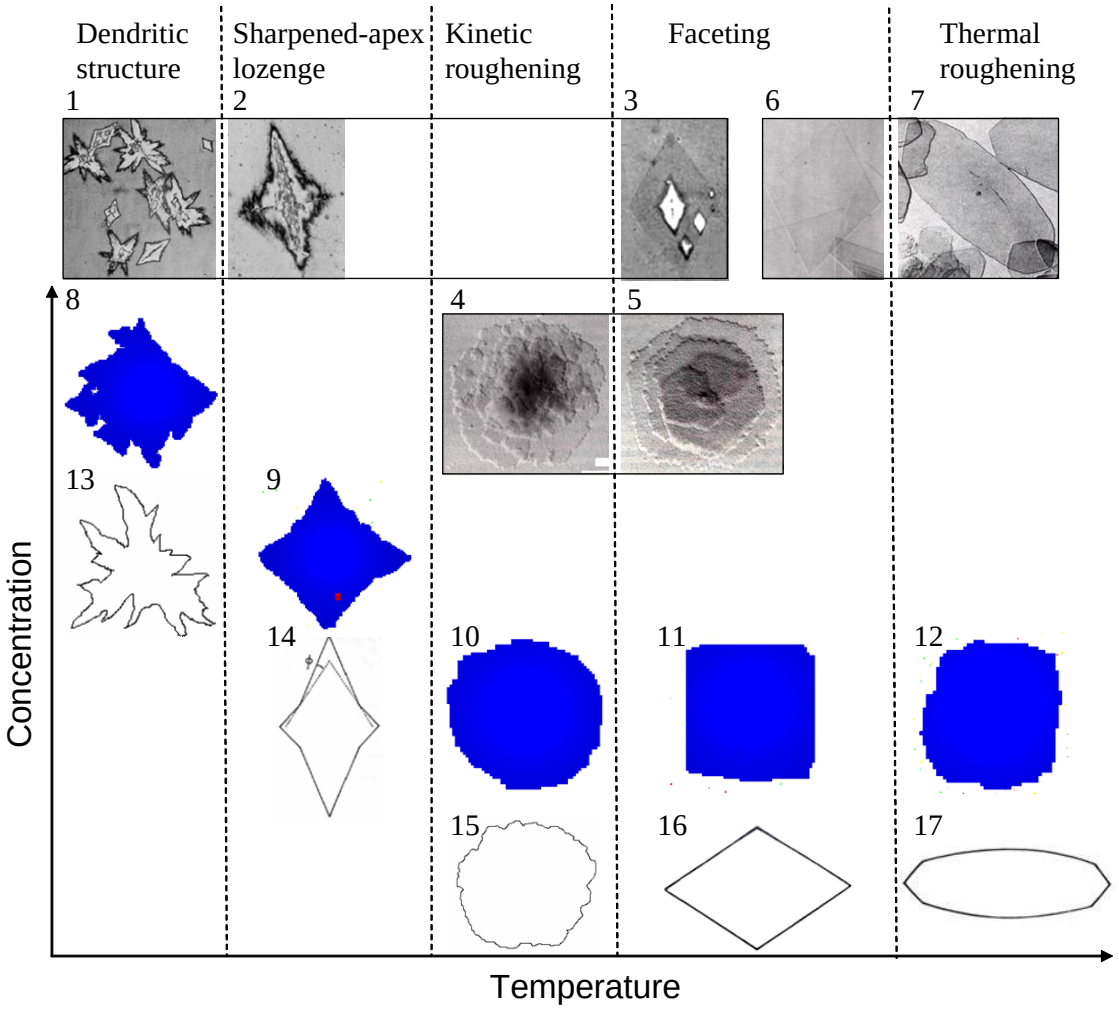

FIG. 3: Schematic representation of five typical habits of solution-grown polymer crystals at different temperatures. The upper part (1-7) shows experimental pictures. (1-3) 0.1% polyethylene in o-Xylene solution (from Wunderlich *et al.* [33]): 1⟩ 62℃; 2⟩ 75℃; 3⟩ 84℃. (4-5) 0.1% isotactic polystyrene in dimethyl phthalate solution (from Tanzawa [35]): 4⟩ 110℃; 5⟩ 130℃. (6-7) 0.05% polyethylene solution (from Organ and Keller [38]): 6⟩ xylene $T_c < 70$℃; 7⟩ tetradecanol 111.8℃. The intermediate part (8-12) presents typical simulation results as a function of temperatures at three different concentrations. (8) At high concentration $C = 0.004$ and low crystallization temperature $kT = 0.100$, a dendritic structure is formed. (9) At intermediate concentration $C = 0.0005$ and low $kT = 0.090$, a sharpened-apex lozenge is formed. (10-12) At low concentration $C = 0.00002$, rough-flat-rough transition occurs with increasing temperature: 10⟩ $kT = 0.100$ kinetic roughening; 11⟩ $kT = 0.135$ faceting; 12⟩ $kT = 0.155$ thermal roughening. The lower part (13-17) gives the corresponding sketches of habits observed in experiments. (14) from Toda and Kiho [34]; (16-17) from Organ and Keller [38]; (13,15) sketches of micrographs (1,4) by ourselves.

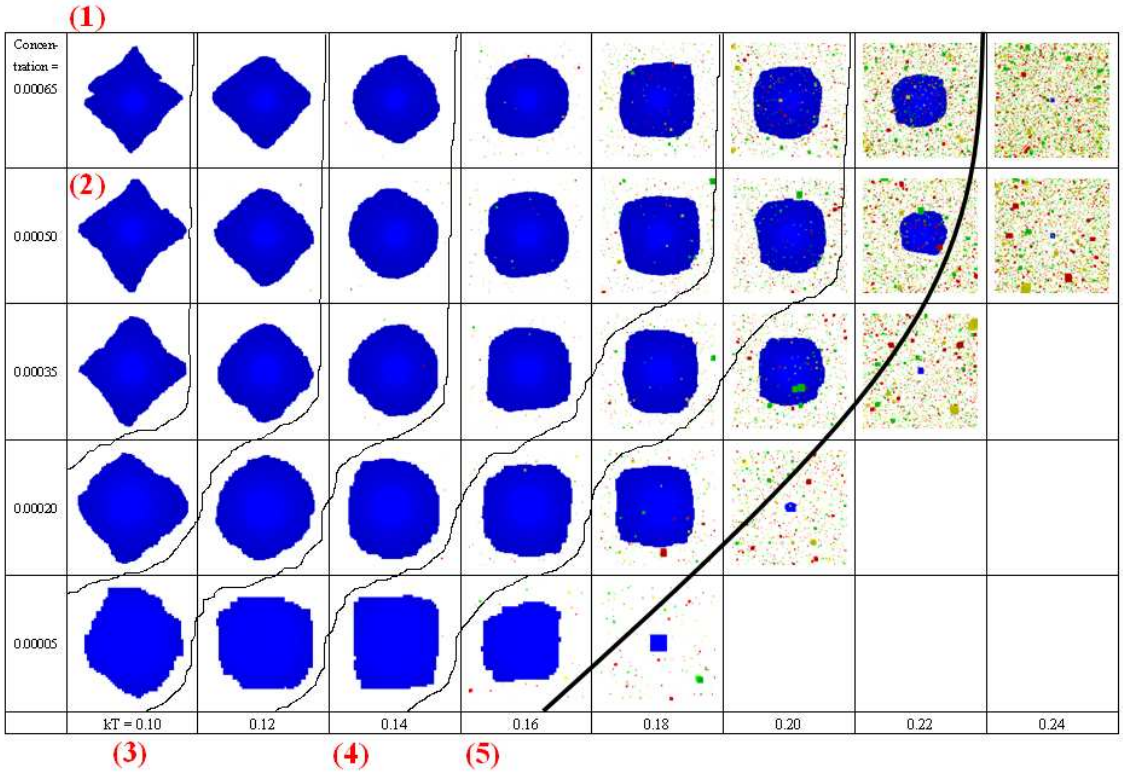

FIG. 4: Full landscape of lateral habits as a function of equally-spaced temperatures and concentrations. The initial nucleus size $nu = 7 \times 7$, the length of simulation box $L_{box} = 300$ and the total simulation time $t_{max} = 2 \times 10^7$ MCS. All morphologies have reached equilibrium at this time step. To maximize the observations, each row of micrographs at different concentrations has been magnified by different ratios. The bold solid line delineate the solubility boundary. If shifting this line toward left, all morphologies along the solid lines are similar. The five typical morphologies shown in Fig. 3 are at the positions (1) $\sim$ (5) in this full landscape.

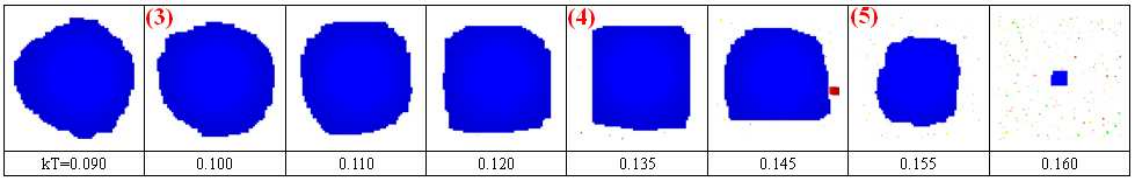

FIG. 5: Rough-flat-rough transition in very dilute polymer solution, where kinetic roughening and thermal roughening are obtained by lowering or increasing temperature respectively. Very low concentration $C = 0.00002$, $L_{box} = 500$, $nu = 7 \times 7$, and $t_{max} \geq 5 \times 10^7$ MCS. All morphologies have reached equilibrium at this time step.

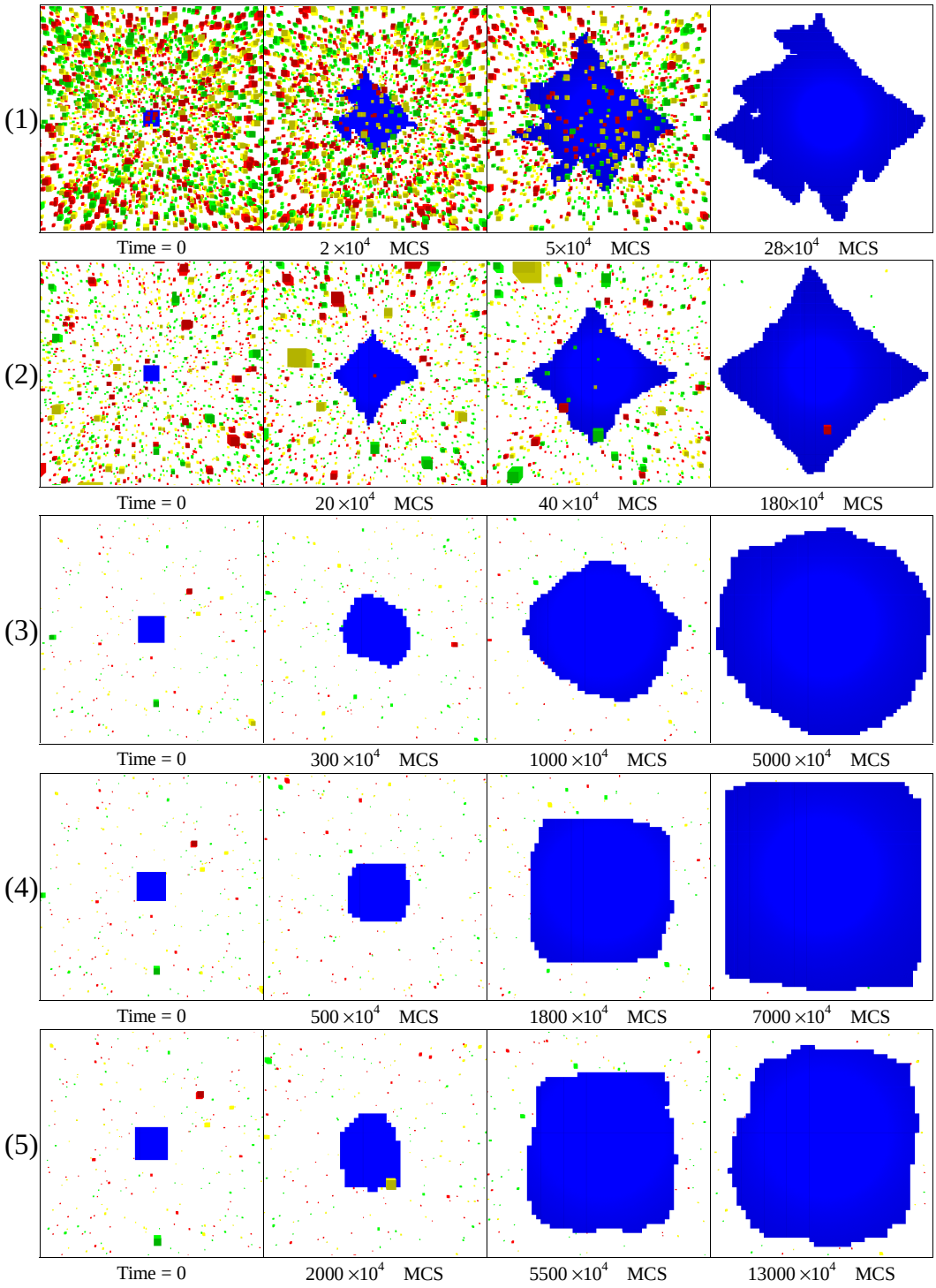

FIG. 6: Time evolution of five typical morphologies in Fig. 3-5. The initial nucleus sizes are the same for case (1)-(5) and $nu = 7 \times 7$. The nuclei may look, however, different in size as a result of being magnified at different ratios. (1) dendritic structure: $C = 0.004$, $kT = 0.100$, $L_{box} = 100$. (2) sharpened-apex lozenge: $C = 0.0005$, $kT = 0.090$, $L_{box} = 200$. (3-5) dilute $C = 0.00002$ and bigger simulation box $L_{box} = 500$: (3) $kT = 0.100$ kinetic roughening; (4) $kT = 0.135$ faceting; (5) $kT = 0.155$ thermal roughening.

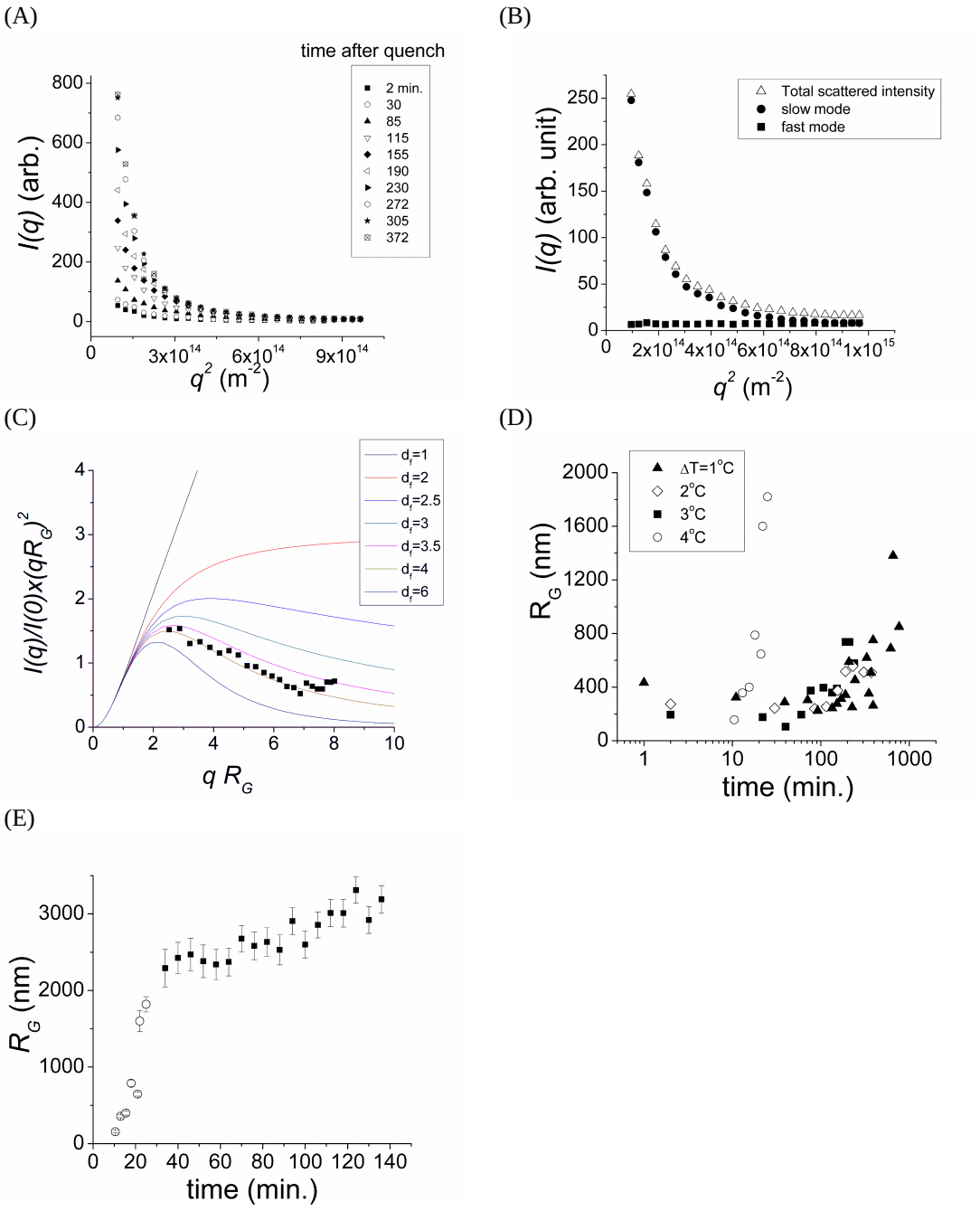

FIG. 7: figure 8

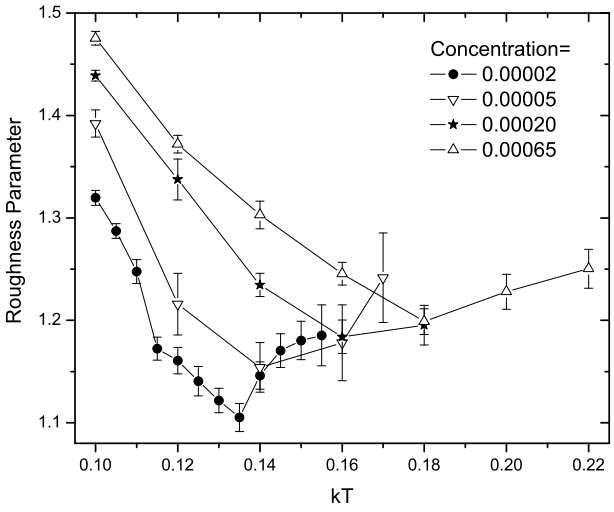

FIG. 8: Plots of roughness (the average number of unmade bonds along x,y directions per edge crystallite) as a function of temperature and concentration. The roughness parameters for $C \geq 0.00005$ are based on morphologies in Fig. 4 and averaged over $100 \sim 200 \times 10^5$ MCS. The roughness parameter for $C = 0.00002$ is based on morphologies in Fig. 5 and averaged over $time = 500 \sim 1000 \times 10^5$ MCS.

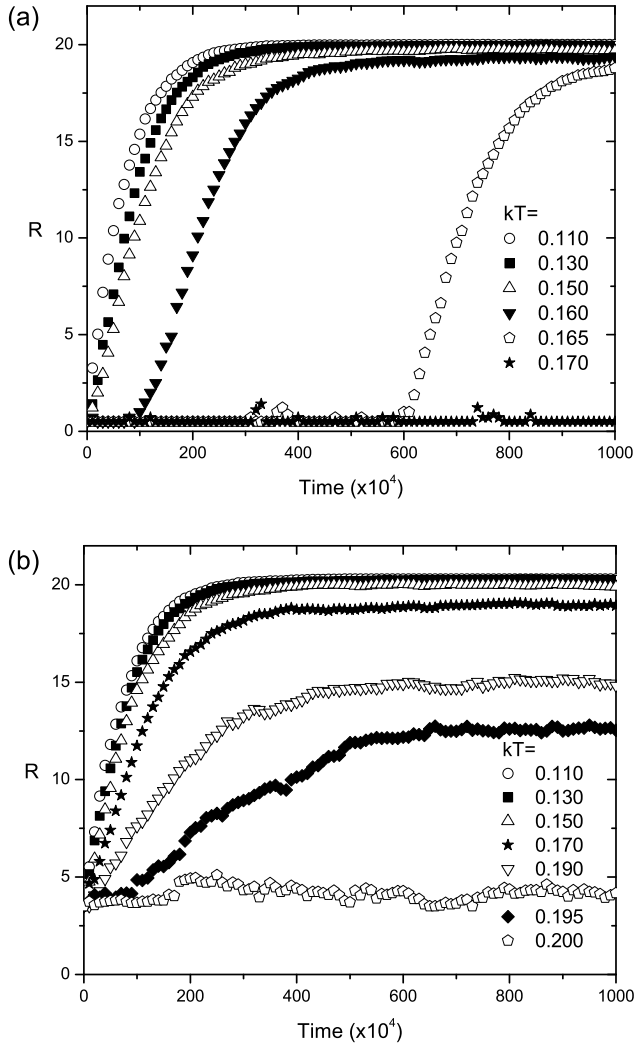

FIG. 9: Time evolution of lamellar radii at various temperatures. $C = 0.0002$, $L_{box} = 200$. (a) the initial nucleus size $nu = 1 \times 1$. (b) $nu = 7 \times 7$.

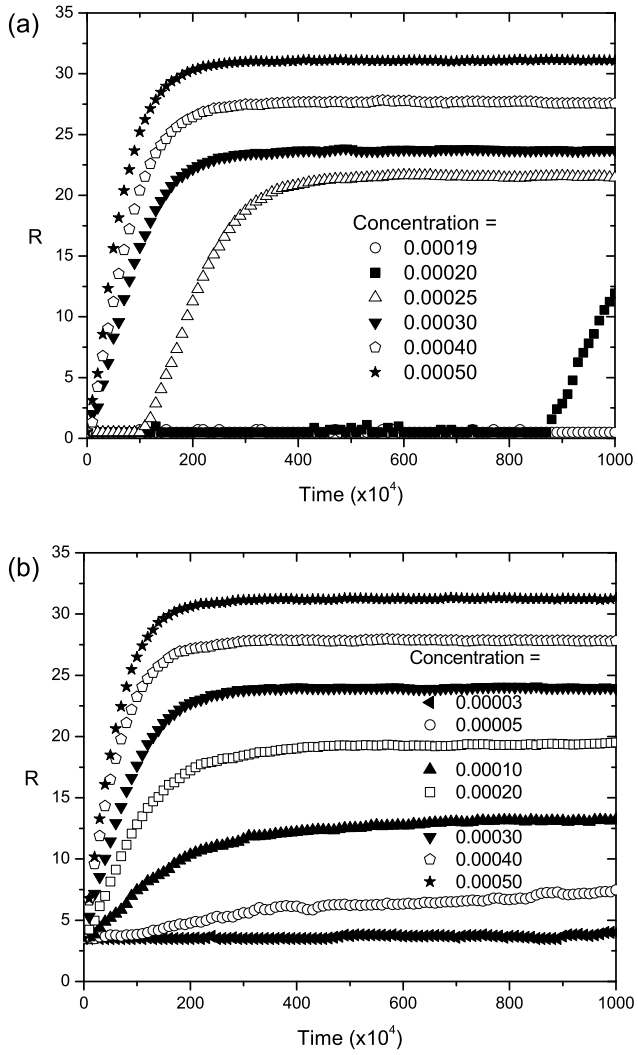

FIG. 10: Time evolution of lamellar radii at various concentrations. $kT = 0.165$, $L_{box} = 200$. (a) the initial nucleus size $nu = 1 \times 1$. (b) $nu = 7 \times 7$.

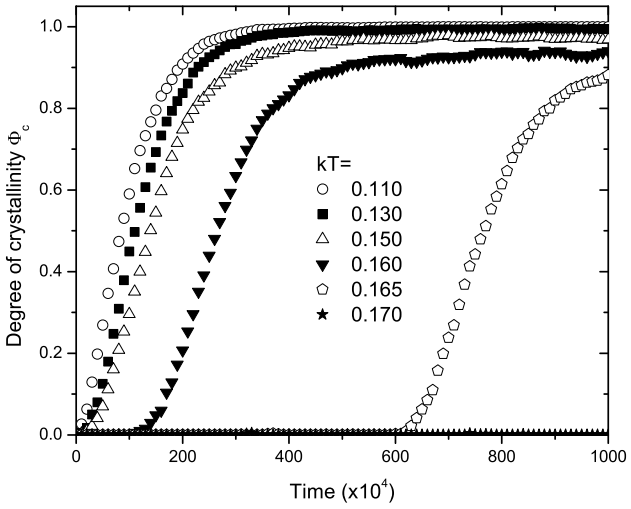

FIG. 11: Time evolution of degree of crystallinity at various temperatures. $C = 0.0002$, $L_{box} = 200$, $nu = 1 \times 1$.

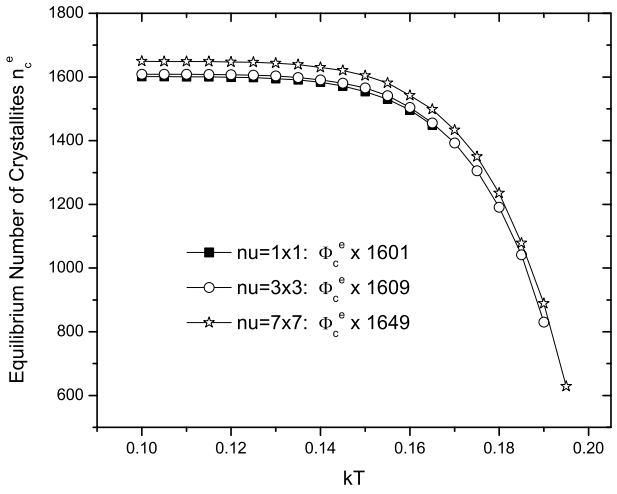

FIG. 12: Temperature dependence of the equilibrium number of crystallites n_c^e, which is proportional to the equilibrium crystallinity Φ_c^e. $C = 0.0002$, $L_{box} = 200$.

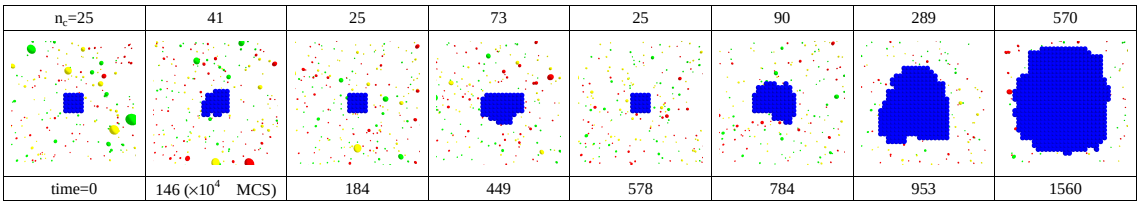

FIG. 13: Nucleation process of the crystal growth. n_c is the total number of crystallites. The initial nucleus size $nu = 5 \times 5$, $C = 0.0002$, $kT = 0.196$, and $L_{box} = 200$.

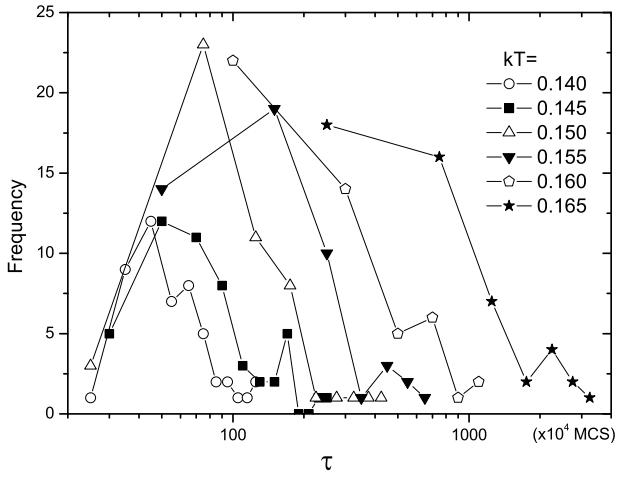

FIG. 14: Log normal distribution of induction times at various temperatures based on 50 runs. $nu = 1 \times 1$, $C = 0.0002$, and $L_{box} = 200$.

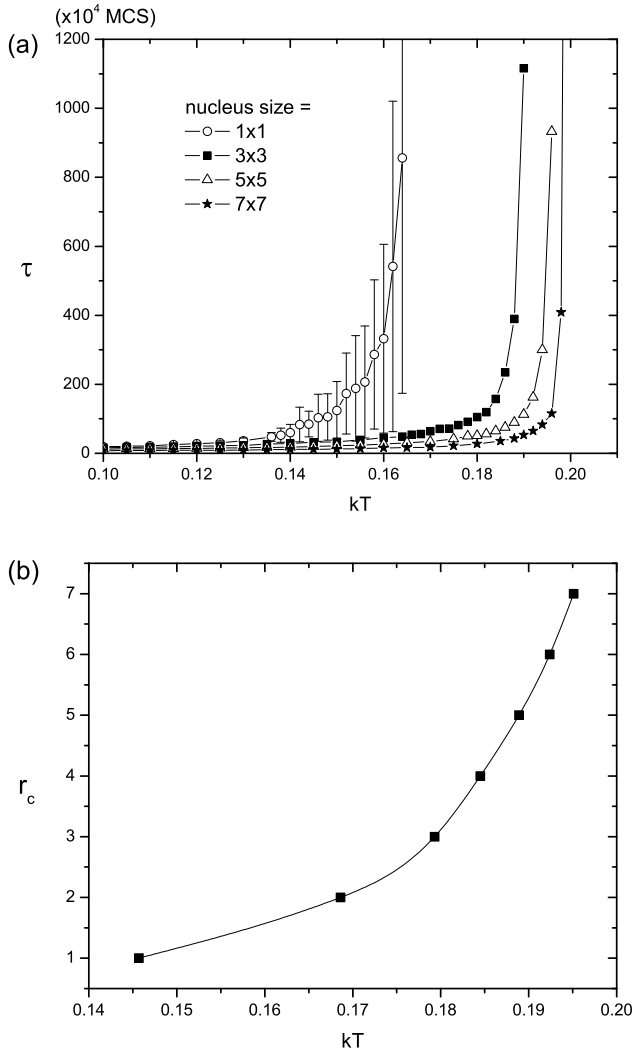

FIG. 15: (a) Induction time τ vs. temperature kT for various initial nucleus size nu. $L_{box} = 200$ and $C = 0.0002$. For the purpose of clarity, the error bar with standard deviation is only shown for the case $nu = 1 \times 1$. (b) Critical nucleus size r_c as a function of temperature kT. This is obtained by intersects of horizontal line $\tau = 100 \times 10^4$ MCS with curves in Fig. 15(a).

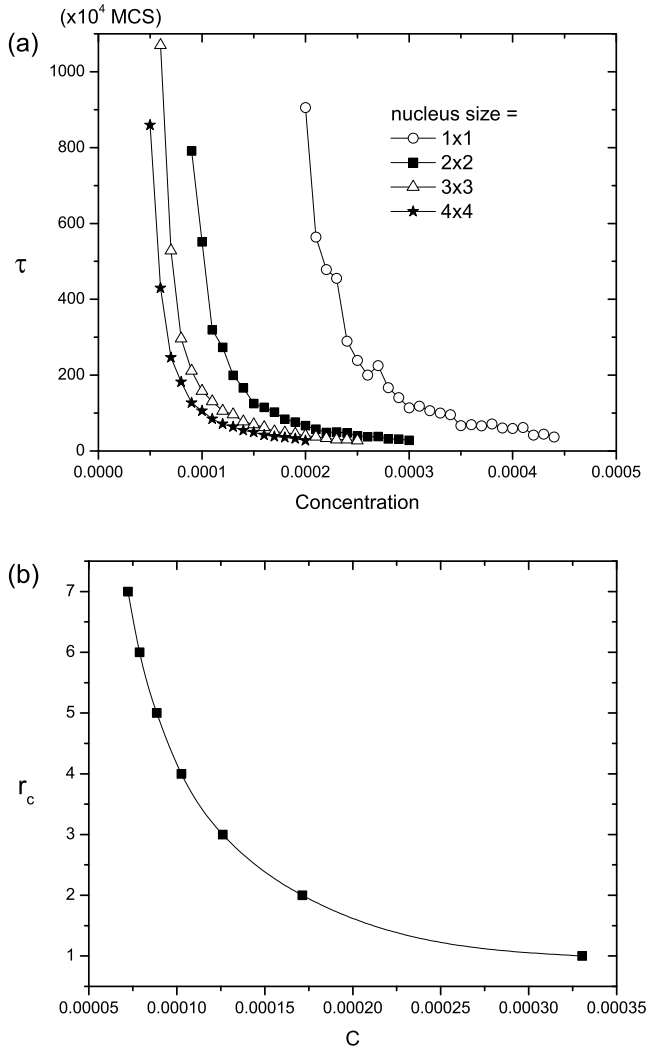

FIG. 16: (a) Induction time τ vs. polymer concentration C for various initial nucleus size nu. $L_{box} = 200$ and $kT = 0.165$. The error bars resemble those in Fig. 15 and not shown here for the purpose of clarity. (b) Critical nucleus size r_c as a function of concentration C. This is obtained by intersects of horizontal line $\tau = 100 \times 10^4$ MCS with curves in Fig. 16(a).

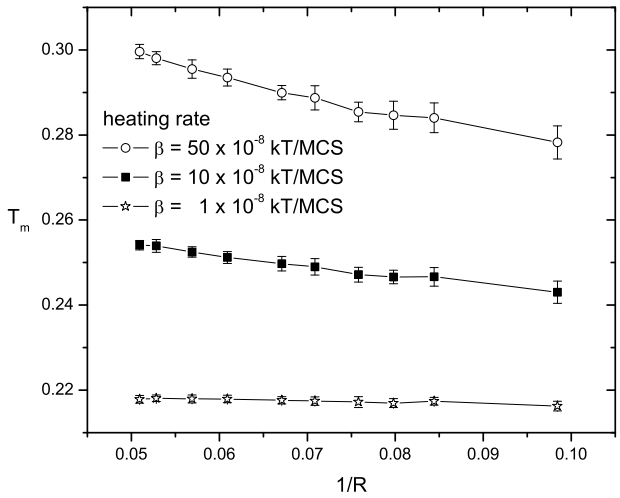

FIG. 17: Gibbs-Thompson thermodynamic equation which relates the melting point T_m with the crystal size R. $L_{box} = 200$, $nu = 7 \times 7$, $C = 0.0002$, $t_c = 1 \sim 4 \times 10^7$ MCS to make sure R reaches its equilibrium value. Each data point is averaged over 50 different runs.

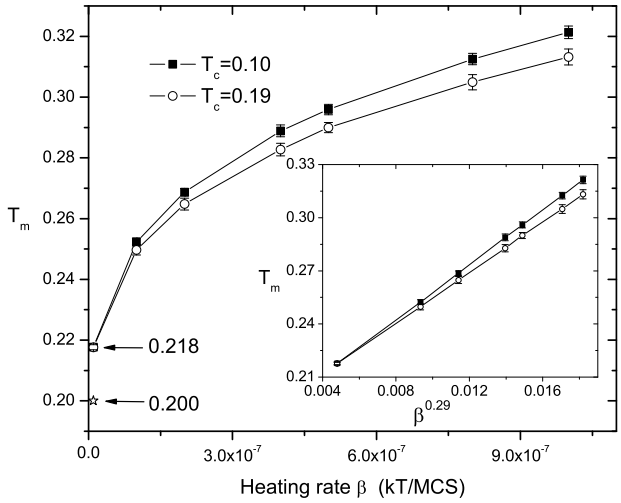

FIG. 18: T_m as a function of heating rate β, indicating superheating effects. $L_{box} = 200$, $nu = 7 \times 7$, $C = 0.0002$, $T_c = 0.10$ or 0.19, $t_c = 5 \sim 10 \times 10^6$ MCS to make sure that simulations reach equilibrium, averaged over 50 runs.

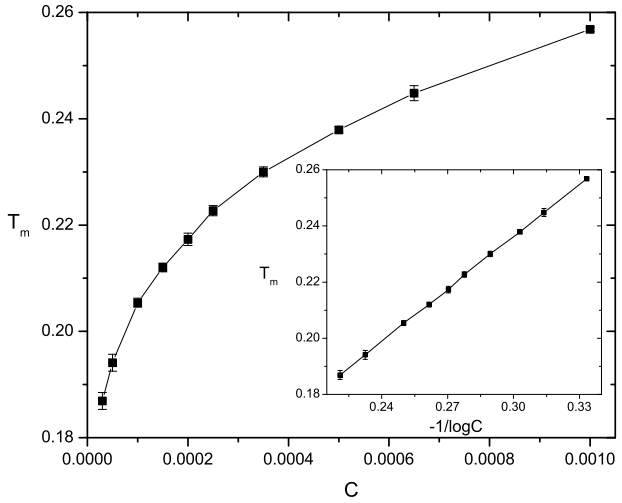

FIG. 19: T_m as a function of polymer concentration C. $L_{box} = 200$, $nu = 7\times7$, $\beta = 1\times10^{-8}$/ MCS, $T_c = 0.100$, $t_c = 1 \times 10^7$ MCS to make sure that simulations reach equilibrium, averaged over 10 runs.

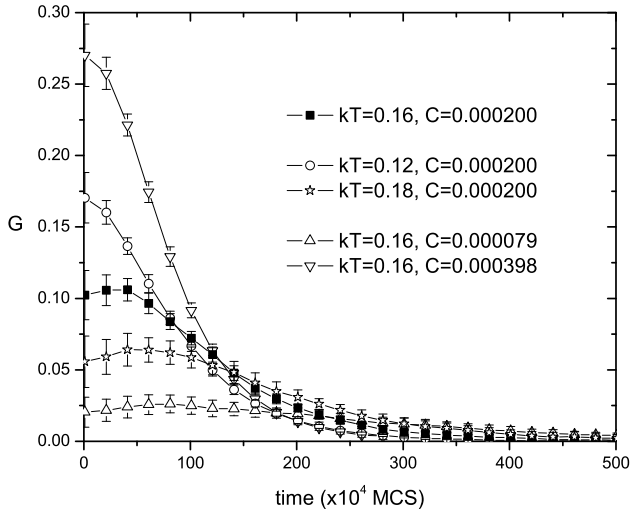

FIG. 20: Variation of the lamellar growth rate G as time elapses. $L_{box} = 200$, $nu = 7\times7$, averaged over 50 runs.

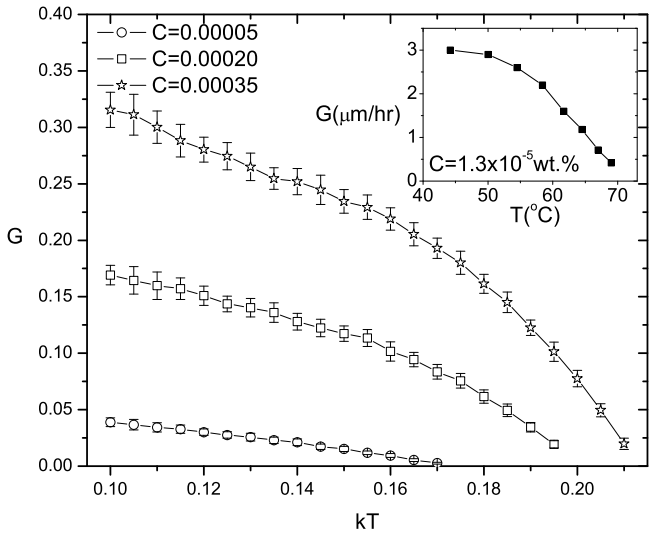

FIG. 21: Temperature dependence of the lamellar growth rate G at various concentrations. $L_{box} = 200$, $nu = 7 \times 7$, averaged over 50 runs. The inset shows experimental data for polyethylene in very dilute solution (from Toda and Kiho, Table II in Ref. [34]), where sharpened-point single crystal was formed.

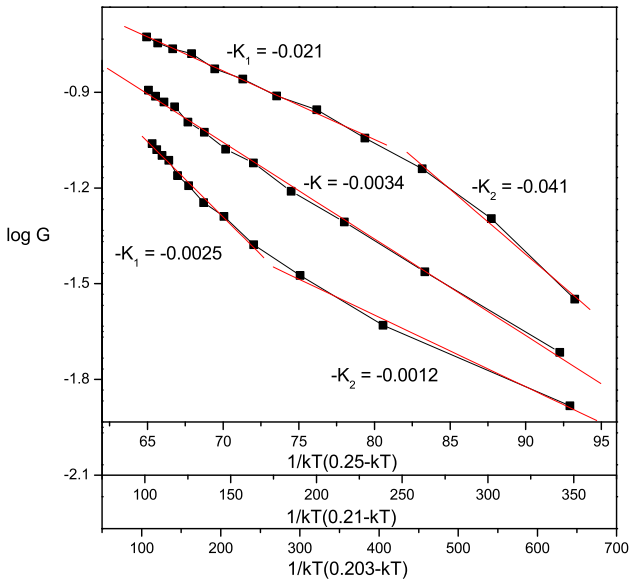

FIG. 22: Replot of $C = 0.00020$ data from Fig. 21 in the form of $\log G$ vs. $1/T(T_m^0 - T)$, where different T_m^0 values have been tried.

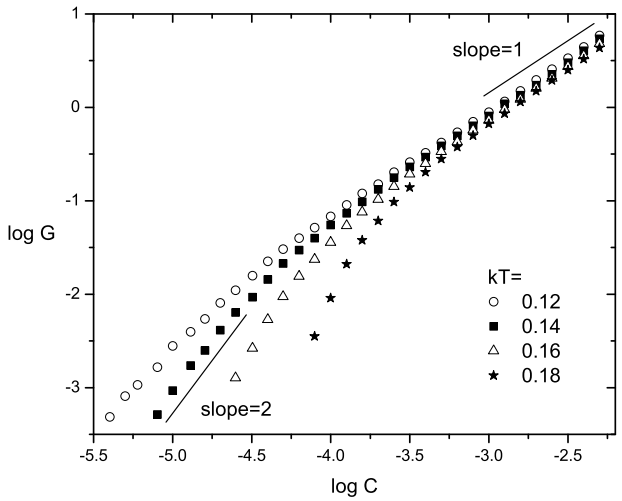

FIG. 23: Concentration dependence of the lamellar growth rate G at various temperatures. $L_{box} = 200$, $nu = 7 \times 7$, averaged over 50 runs.

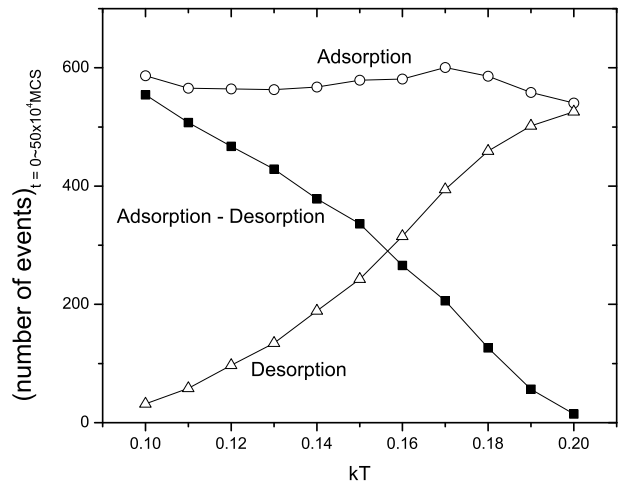

FIG. 24: The total number of adsorption/desorption events occurred during the early stage of crystallization at various temperatures. Note (Adsorption - Desorption) is equal to the lamellar growth rate. $L_{box} = 200$, $nu = 7 \times 7$, $C = 0.0002$.

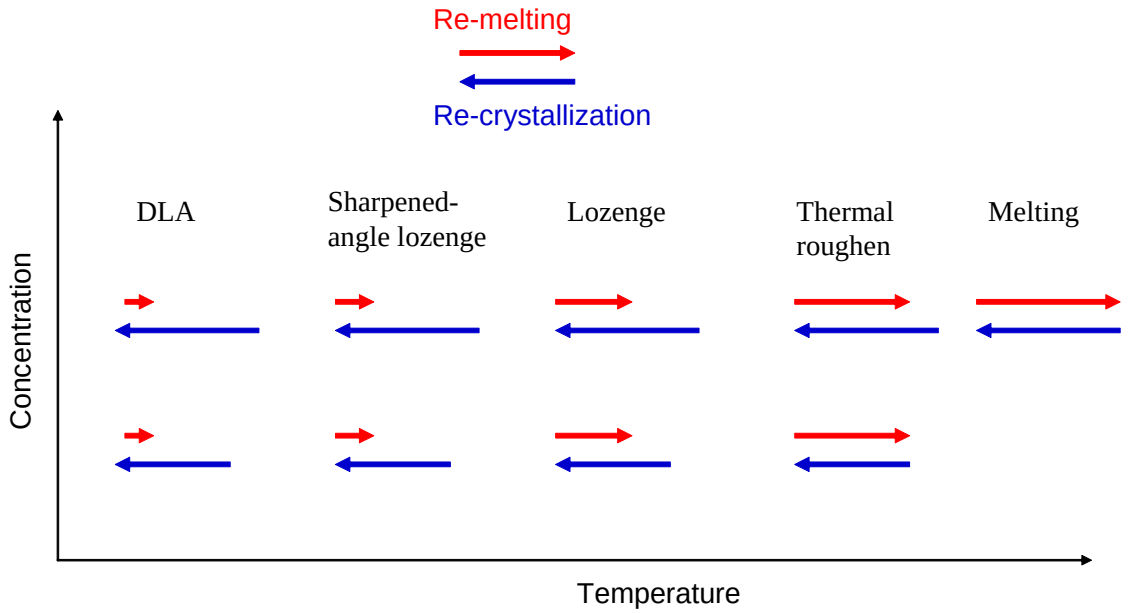

FIG. 25: Reversible crystallization/melting and resultant morphologies as a function of temperature and concentrations.

(a)

2	3	2
3	4	3
2	3	2

(b)

2	3	3	3	2
3	4	4	4	3
3	4	4	4	3
3	4	4	4	3
2	3	3	3	2

FIG. 26: Mechanism of nucleation and surface energy. (a) 3×3 nucleus (b) 5×5 nucleus. The number in each square designates how many neighboring crystallites it has.